COMPARATIVE ASSESSMENT OF A TWO-LAYERED AND MULTI-LAYERED SEDIMENT MODEL

by

Robin Francois Dean Wilson

Submitted in partial fulfillment of the requirements
for the degree of Master of Science

at

Dalhousie University
Halifax, Nova Scotia
September 2011

DALHOUSIE UNIVERSITY

DEPARTMENT OF OCEANOGRAPHY

The undersigned hereby certify that they have read and recommend to the Faculty of Graduate Studies for acceptance a thesis entitled "COMPARATIVE ASSESSMENT OF A TWO-LAYERED AND MULTI-LAYERED SEDIMENT MODEL" by Robin Francois Dean Wilson in partial fulfillment of the requirements for the degree of Master of Science.

Dated: September 1, 2011

External Examiner: _____

Supervisor: _____

Readers: _____

_____

_____

DALHOUSIE UNIVERSITY

DATE: September 1, 2011

AUTHOR: Robin Francois Dean Wilson

TITLE: COMPARATIVE ASSESSMENT OF A TWO-LAYERED AND MULTI-LAYERED SEDIMENT MODEL

DEPARTMENT OR SCHOOL: Department of Oceanography

DEGREE: M.Sc. CONVOCATION: May YEAR: 2012

_____

Signature of Author

To my wife, who would probably rather read Harry Potter. But that's fine. I would prefer the same.

TABLE OF CONTENTS

LIST OF TABLES

LIST OF FIGURES

ABSTRACT

Coastal sediments continuously interact with the overlying water column, collecting and decomposing the incoming rain of organic detritus into inorganic nutrients, and consuming oxygen in the process. This thesis compares the ability of two qualitatively different sediment models, a two-layer and a multi-layer model, to quantify the biogeochemical transformations that occur when detritus is decomposed in the sediment. Using sediment flux observations from a mesocosm eutrophication experiment, selected model parameters and different parameterizations for depositional fluxes of organic matter have been optimized using an evolutionary algorithm and a gradient descent algorithm respectively. Simulations with constant depositional fluxes outperformed simulations where deposition was dependent on proxies of biomass concentration in the overlying water. With these constant inputs, both sediment models produced similar nutrient fluxes across the sediment-water interface, however the multi-layer model was better able to adapt to new environments.

LIST OF ABBREVIATIONS AND SYMBOLS USED

General Notation:

Symbol	Description	Units
C	Concentration	$\frac{\mu\mathrm{mol}}{\mathrm{cm}^3}$
R	Reaction rate	$\frac{\mu\mathrm{mol}}{\mathrm{cm}^3\mathrm{d}}$
$R^\star$	Vertically integrated reaction rate	$\frac{\mu\mathrm{molC}}{\mathrm{cm}^2\mathrm{d}}$
J	Flux	$\frac{\mu\mathrm{molC}}{\mathrm{cm}^2\mathrm{d}}$
L	Mass transfer coefficient	$\frac{\mathrm{cm}}{\mathrm{d}}$
r	Specific rate constant	$\frac{1}{\mathrm{d}}$
D	Diffusion constant	$\frac{\mathrm{cm}^2}{\mathrm{d}}$
k	Half saturation constant	$\frac{\mu\mathrm{mol}}{\mathrm{cm}^3}$

Calculated quantities:

Symbol	Description	Units
$R^\star_{\mathrm{tot,C}}$	Total sediment carbon consumption rate, vertically integrated	$\frac{\mu\mathrm{molC}}{\mathrm{cm}^2\mathrm{d}}$
$R^\star_{\mathrm{aer,C}}$	Aerobic carbon consumption rate, vertically integrated	$\frac{\mu\mathrm{molC}}{\mathrm{cm}^2\mathrm{d}}$
$R^\star_{\mathrm{dnf,C}}$	Denitrification carbon consumption rate, vertically integrated	$\frac{\mu\mathrm{molC}}{\mathrm{cm}^2\mathrm{d}}$
$R^\star_{\mathrm{nit,O_2}}$	Nitrification oxygen consumption rate, vertically integrated	$\frac{\mu\mathrm{molO}}{\mathrm{cm}^2\mathrm{d}}$
J_i	Outflux of substance i from sediment, $i = \{\mathrm{O_2}, \mathrm{NH_4}, \mathrm{NO_3}, \mathrm{PO_4}\}$	$\frac{\mu\mathrm{mol}}{\mathrm{cm}^2\mathrm{d}}$
$\bar{J}_\mathrm{i}$	Time averaged benthic flux of substance $i = \{\mathrm{O_2}, \mathrm{NH_4}, \mathrm{NO_3}, \mathrm{PO_4}\}$	$\frac{\mu\mathrm{mol}}{\mathrm{cm}^2\mathrm{d}}$
$[\mathrm{C}]$	Sediment concentration, organic carbon	$\frac{\mu\mathrm{molC}}{\mathrm{cm}^3}$
$[\mathrm{O_2}]$	Porewater concentration, oxygen	$\frac{\mu\mathrm{molO}}{\mathrm{cm}^3}$
$[\mathrm{NO_3}]$	Porewater concentration, nitrate/nitrite	$\frac{\mu\mathrm{molN}}{\mathrm{cm}^3}$
$[\mathrm{NH_4}]$	Porewater concentration, ammonium	$\frac{\mu\mathrm{molN}}{\mathrm{cm}^3}$
$[\mathrm{PO_4}]$	Porewater concentration, phosphate	$\frac{\mu\mathrm{molP}}{\mathrm{cm}^3}$

Two-Layer Model:

Symbol	Description	Units
$[\mathrm{C}]_j$	Organic carbon in layer $j = \{1, 2\}$	$\frac{\mu\mathrm{molC}}{\mathrm{cm}^3}$
$[\mathrm{O_2}]_j$	Oxygen in layer $j = \{\mathrm{olwc}, 1, 2\}$	$\frac{\mu\mathrm{molO}}{\mathrm{cm}^3}$
$[\mathrm{NO_3}]_j$	Nitrate carbon in layer $j = \{\mathrm{olwc}, 1, 2\}$	$\frac{\mu\mathrm{molN}}{\mathrm{cm}^3}$
$[\mathrm{NH_4}]_j$	Ammonium in layer $j = \{\mathrm{olwc}, 1, 2\}$	$\frac{\mu\mathrm{molN}}{\mathrm{cm}^3}$
$[\mathrm{PO_4}]_j$	Phosphate in layer $j = \{\mathrm{olwc}, 1, 2\}$	$\frac{\mu\mathrm{molP}}{\mathrm{cm}^3}$
S	Benthis stress	-
R_{met}	Sediment carbon metabolic rate of a given layer	$\frac{\mu\mathrm{molC}}{\mathrm{cm}^3\mathrm{d}}$
R_{dnf}	Denitrification rate of a given layer	$\frac{\mu\mathrm{molC}}{\mathrm{cm}^3\mathrm{d}}$
R_{nit}	Nitrification rate	$\frac{\mu\mathrm{molC}}{\mathrm{cm}^3\mathrm{d}}$
$R^{\star}_{\mathrm{SOD}}$	Sediment oxygen demand	$\frac{\mu\mathrm{molO}}{\mathrm{cm}^2\mathrm{d}}$
$R^{\star}_{\mathrm{CSOD}}$	Sediment oxygen demand due to the oxidation of carbon, $\mathrm{H_2S}$, and $\mathrm{CH_4}$	$\frac{\mu\mathrm{molO}}{\mathrm{cm}^2\mathrm{d}}$
$R^{\star}_{\mathrm{NSOD}}$	Sediment oxygen demand due to nitrification	$\frac{\mu\mathrm{molO}}{\mathrm{cm}^2\mathrm{d}}$
$R_{\mathrm{src},j}$	Chemical source for a substance in layer $j = \{1, 2\}$	$\frac{\mu\mathrm{mol}}{\mathrm{cm}^3\mathrm{d}}$
$R_{\mathrm{snk},j}$	Chemical sink for a substance in layer $j = \{1, 2\}$	$\frac{\mu\mathrm{mol}}{\mathrm{cm}^3\mathrm{d}}$
$L_{i,j}$	Mass transfer coefficient between layers $i, j = \{\mathrm{olwc}, 1, 2\}$	$\frac{\mathrm{cm}}{\mathrm{d}}$
L_{sed}	Mass transfer coefficient due to burial	$\frac{\mathrm{cm}}{\mathrm{d}}$
H_j	Thickness of layer $j = \{1, 2\}$	cm
D_{pw}	Porewater diffusion rate constant	$\frac{\mathrm{cm}^2}{\mathrm{d}}$
D_{s}	Bioturbation, base diffusion rate constant	$\frac{\mathrm{cm}^2}{\mathrm{d}}$
$\theta_{\mathrm{D_{pw}}}$	Porewater diffusion temperature correction	-
$\theta_{\mathrm{D_s}}$	Bioturbation temperature correction	-
$r_{\mathrm{met},\ell}$	Carbon decay specific rate constant for lability class ℓ = { 1,2,3}	$\frac{1}{d}$
$r_{\mathrm{dnf},j}$	Specific rate constant for denitrification in layer j = {1, 2}	$\frac{1}{d}$
r_{nit}	Specific rate constant for nitrification	$\frac{1}{d}$
$r_{\mathrm{H_2Sox},i}$	Specific rate constant for sulfide oxidation, phase i = {aq,s}, i.e. aqueous and solid phases	$\frac{1}{d}$
$r_{\mathrm{CH_4ox}}$	Specific rate constant for methane oxidation	$\frac{1}{d}$
r_{st}	Benthic stress decay rate	$\frac{1}{d}$

Symbol	Description	Units
$\theta_{\mathrm{met},\ell}$	Approximated Arrhenius factor for carbon metabolism, lability class ℓ = { 1,2,3}	-
$\theta_{\mathrm{dnf},j}$	Approximated Arrhenius factor for denitrification in layer j = $\{1, 2\}$	-
θ_{nit}	Approximated Arrhenius factor for nitrification	-
$\theta_{\mathrm{H_2Sox}}$	Approximated Arrhenius factor for sulfide oxidation	-
$\theta_{\mathrm{CH_4ox}}$	Approximated Arrhenius factor for methane oxidation	-
$k_{\mathrm{nit,NH_4}}$	Nitrification, NH_4 half saturation	$\frac{\mu molN}{cm^3}$
$k_{\mathrm{nit,O_2}}$	Nitrification, O_2 half saturation	$\frac{\mu molO}{cm^3}$
$k_{\mathrm{H_2Sox}}$	Sulfide oxidation, O_2 normalization constant	$\frac{\mu molO}{cm^3}$
$k_{\mathrm{CH_4ox}}$	Methane oxidation, O_2 half saturation constant	$\frac{\mu molO}{cm^3}$
$\pi_{\mathrm{PO4,base}}$	Partition parameter, base	$\frac{\mathrm{cm^3(solid)}}{\mathrm{cm^3(porewater)}}$
$\pi_{\mathrm{PO4,exp}}$	Partition coefficient, exponential	-
$[\mathrm{O_2}]_{\mathrm{crit}}$	Phosphate partitioning, critical oxygen concentration	$\frac{\mu\mathrm{molO}}{\mathrm{cm^3}}$
H_j	Thickness of layer j = {1,2}	cm
$H_{\mathrm{SO_4}}$	Thickness of sulphate layer	cm

Multi-Layer Model:

Symbol	Description	Units
$[\mathrm{C}]_\ell$	Organic carbon, lability class $\ell = \{1, 2\}$	$\frac{\mu\mathrm{molC}}{\mathrm{cm^3}}$
$[\mathrm{O_2}]$	Oxygen	$\frac{\mu\mathrm{molO}}{\mathrm{cm^3}}$
$[\mathrm{NO_3}]$	Nitrate	$\frac{\mu\mathrm{molN}}{\mathrm{cm^3}}$
$[\mathrm{NH_4}]$	Ammonium	$\frac{\mu\mathrm{molN}}{\mathrm{cm^3}}$
R_{met}	Sediment carbon metabolic rate of a given layer	$\frac{\mu\mathrm{molC}}{\mathrm{cm^3d}}$
R_{nit}	Nitrification rate of a given layer	$\frac{\mu\mathrm{molC}}{\mathrm{cm^3d}}$
R_{ODUox}	ODU oxidation rate of a given layer	$\frac{\mu\mathrm{molO_2}}{\mathrm{cm^3d}}$
$R_{\mathrm{src},j}$	Chemical source for a substance in layer $j = \{1, 2\}$	$\frac{\mu\mathrm{mol}}{\mathrm{cm^3d}}$
$R_{\mathrm{snk},j}$	Chemical sink for a substance in layer $j = \{1, 2\}$	$\frac{\mu\mathrm{mol}}{\mathrm{cm^3d}}$
$r_{\mathrm{met},\ell}$	Carbon decay specific rate constant for lability class ℓ = { 1,2}	$\frac{1}{d}$
$r_{\mathrm{dnf},j}$	Specific rate constant for denitrification in layer j = $\{1, 2\}$	$\frac{1}{d}$
r_{nit}	Specific rate constant for nitrification	$\frac{1}{d}$

Symbol	Description	Units
$r_{\mathrm{H_2Sox},i}$	Specific rate constant of sulfide oxidation for phases i = {aq,s}, i.e. aqueous and solid phases	$\frac{1}{d}$
$r_{\mathrm{CH_4ox}}$	Specific rate constant for methane oxidation	$\frac{1}{d}$
v_{sed}	Sedimentation rate	$\frac{\mathrm{cm}}{\mathrm{d}}$
D_{pw}	Porewater diffusion rate constant	$\frac{\mathrm{cm}^2}{\mathrm{d}}$
D_{s}	Bioturbation, base diffusion rate constant	$\frac{\mathrm{cm}^2}{\mathrm{d}}$
$\theta_{\mathrm{D_{pw}}}$	Porewater diffusion temperature correction	-
$\theta_{\mathrm{D_s}}$	Bioturbation temperature correction	-
$\theta_{\mathrm{met},\ell}$	Approximated Arrhenius factor for carbon metabolism, lability class ℓ = { 1,2,3}	-
θ_{k,nit,NH_4}	Nitrification NH_4 temperature sensitivity factor	-
$k_{\mathrm{nit,NH_4}}$	Nitrification, NH_4 half saturation	$\frac{\mu molN}{cm^3}$
$k_{\mathrm{nit,O_2}}$	Nitrification, O_2 half saturation	$\frac{\mu molO}{cm^3}$
$k_{\mathrm{H_2Sox}}$	ODU oxidation, O_2 half saturation constant	$\frac{\mu molO}{cm^3}$
$k_{\mathrm{aer,O_2}}$	Aerobic oxidation, O_2 half saturation constant	$\frac{\mu molO}{cm^3}$
$k_{\mathrm{dnf,O_2}}$	Denitrification O_2 inhibition constant	$\frac{\mu molO}{cm^3}$
$k_{\mathrm{dnf,NO_3}}$	Denitrification NO_3 inhibition constant	$\frac{\mu molN}{cm^3}$
$k_{\mathrm{anox,O_2}}$	Anaerobic metabolism, O_2 inhibition constant	$\frac{\mu molO}{cm^3}$
$k_{\mathrm{anox,NO_3}}$	Anaerobic metabolism, NO_3 inhibition constant	$\frac{\mu molN}{cm^3}$
lim_{aer}	Aerobic limitation term	-
lim_{dnf}	Denitrification limitation term	-
lim_{anox}	Anaerobic limitation term	-

POM Flux Parameterizations:

Symbol	Description	Units
J_{POM}	Depositional flux of particulate organic matter	$\frac{\mu\mathrm{molC}}{\mathrm{cm}^2\mathrm{d}}$
$[Chl]$	Chlorophyll concentration	$\frac{\mu\mathrm{gchl}}{\mathrm{L}}$
$[Zoo]$	Zooplankton concentration	$\frac{\mu\mathrm{gchl}}{\mathrm{L}}$
$[\mathrm{A}]_{\mathrm{dia}}$	Abundance of diatoms	$\frac{\mathrm{number}}{\mathrm{L}}$
$[\mathrm{A}]_{\mathrm{tot}}$	Total abundance of diatoms	$\frac{\mathrm{number}}{\mathrm{L}}$
p_{const}	Method A, constant flux of particulate organic matter	$\frac{\mu\mathrm{molC}}{\mathrm{cm}^2\mathrm{d}}$
p_{chla}	Method B, constant of proportionality	$\frac{\mu\mathrm{molC}}{\mathrm{cm}^2\mathrm{d}}\frac{\mathrm{L}}{\mu\mathrm{gchl}}$

Symbol	Description	Units
p_{dia}	Method C, depositional flux constant of proportionality	$\frac{\mu\mathrm{molC}}{\mathrm{cm}^2\mathrm{d}}\frac{\mathrm{L}}{\mu\mathrm{gchl}}$
p_{other}	Method C, depositional flux, constant of proportionality	$\frac{\mu\mathrm{molC}}{\mathrm{cm}^2\mathrm{d}}\frac{\mathrm{L}}{\mu\mathrm{gchl}}$
p_{chla}	Method D, depositional flux, constant of proportionality	$\frac{\mu\mathrm{molC}}{\mathrm{cm}^2\mathrm{d}}\frac{\mathrm{L}}{\mu\mathrm{gchl}}$
p_{zoo}	Method D, depositional flux, constant of proportionality	$\frac{\mu\mathrm{molC}}{\mathrm{cm}^2\mathrm{d}}\frac{\mathrm{L}}{\mathrm{dry}\mu\mathrm{g}}$
F	Cost function	-
$\vec{p}$	Model parameter set	-
$X_{\mathrm{m}}^{\mathrm{obs}}$	Observation of data type m = $\{O_2, NO_3, NH_4, PO_4\}$	-
$X_{\mathrm{m}}^{\mathrm{mod}}$	Model output for data type m = $\{O_2, NO_3, NH_4, PO_4\}$	-
W_m	Cost weighting for data type m = $\{O_2, NO_3, NH_4, PO_4\}$	-
H	Hessian matrix	-

Abbreviations:

Abbreviation	Meaning
MERL	Mesocosm Eutrophication Research Laboritory
olwc	Overlying water column
POM	Particulate organic matter
SSE	Sum of the squared error
ODU	Oxygen deficit unit

ACKNOWLEDGEMENTS

Many thanks to my supervisor, Katja Fennel, for her years of patience, to the members of MEMG for their generous assistance and suggestions, and to my funding agencies, Dalhousie University and NOAA.

CHAPTER 1

INTRODUCTION

At the ocean's bottom, sinking organic detritus is deposited into the sediment, which becomes a focal site of decomposition. Many metabolisms are involved in the process, each functioning according to the availability of oxidizing agents in the environment: aerobic metabolisms react oxygen with organic matter directly; in the absence of oxygen, denitrification reacts organic carbon with nitrate, which is converted into inert N_2 gas; lacking oxygen and nitrate, sulphate is consumed, producing H_2S gas; under anaerobic conditions metal oxides may oxidize organic matter; and finally, failing the availability of any of the above reactants, microbes can convert organic carbon into methane (*Boudreau*, 1997; *Berner*, 1980). Decomposition of organic matter results in the release of nutrients, namely, phosphate (PO_4), inorganic nitrogen (NH_4, NO_3, NO_2), and silica. Further reactions take place when reduced compounds are exposed to oxygen. For example, ammonium is nitrified to nitrate, and H_2S, or a number of other reduced end products of an anaerobic metabolism can become oxidized within aerobic layers of the sediments. Sediment, processes, therefore influence the biogeochemical dynamics of the overlying ocean through the consumption of oxygen and the release of inorganic nutrients.

The importance of sediments to ocean biogeochemistry varies with water depth and vertical circulation rates (*Kemp et al.*, 1992). When waters are shallow, more labile organic matter is able sink to the bottom before being metabolized. Both shallow waters and vertical circulation facilitate the recirculation of remineralized nutrients from the sediments into the photic zone, supporting the uptake of nutrients by photosynthesis. Higher rates of photosynthesis in turn generate more organic matter that can be re-deposited in the

sediments. In sum, shallower waters and higher rates of vertical exchange increase the benthic-pelagic coupling, and thus this coupling is is often pronounced within bays, coastal oceans, and continental shelves. For example, mesocosm experiments have shown sediments in well mixed water of 5m depth to represent over half the system's respiration (*Oviatt et al.*, 1986). Thus, an understanding of these shallow systems' biogeochemical dynamics requires an understanding of sediment chemistry.

When constructing the nitrogen budget of a shallow system, it is critical to estimate rates of denitrification accurately. This reaction converts reactive nitrogen species into the N_2 gas which is biologically inaccessible to all but a few life forms. Thus, denitrification functions to permanently remove nitrogen from the ocean (*Seitzinger et al.*, 2006). Rates of sediment denitrification on coastal and shelf oceans can be high, with some estimates attributing 35-45% of the world's total denitrification to coastal and shelf sediments (*Middelburg et al.*, 1996; *Seitzinger et al.*, 2006). Thus, in order to properly construct global nitrogen budgets, sediment denitrification rates must be quantified.

It is challenging to estimate rates of denitrification as they are subject to a number of environmental factors. For instance, it is more thermodynamically favourable to metabolize organic matter with oxygen than with nitrate, and thus denitrification rates drop when the environment becomes oxygenated. Denitrification also requires a supply of nitrate, which is generated by nitrifying ammonia, and requires oxygen. Therefore, both the absence or excess of oxygen can prevent denitrification from taking place; thus, denitrification primarily occurs in spatial and temporal transitions between oxic and anoxic environments. In many cases, sophisticated models are required to produce accurate denitrification rates, particularly in low oxygen environments (*Kemp et al.*, 1990; *Seitzinger et al.*, 2006).

The inhibition of denitrification in anoxic waters can induce an important feedback on ocean biogeochemistry. If, under anoxic conditions, reactive nitrogen is not removed from the system by denitrification, but accumulates in the form of ammonium instead, it can be oxidized in the overlying water, or transported back to the surface and used for photosynthesis (*Kemp et al.*, 2005). Sediments also exhibit feedbacks of phosphate release under low oxygen conditions. Episodes of suboxic bottom water result in amplified outfluxes of PO_4 (*DiToro*, 2001). The effect is postulated to occur as oxic conditions prompt the sorption of PO_4 to iron oxyhydroxide, which later can release PO_4 should the environment become sufficiently reduced to dissolve this iron compound (*Boström et al.*,

1988). This mechanism has been observed in the sediments of Chesapeake Bay, where bottom waters experience intense seasonal anoxia (*Boesch et al.*, 2001; *Kemp et al.*, 2005).

Low oxygen conditions in shallow systems are often associated with eutrophication, a condition of the water column where high nutrient concentrations stimulate large blooms of phytoplankton. The effects of such a high concentration of water column biomass can induce a wide variety of alterations to the aquatic environment, including bottom water hypoxia. This can happen when the growth of biomass is stimulated near the water surface, and decomposing biomass begins to sink. If the ocean's mixing rate is low, the oxygen demand of the decomposing biomass may outweigh the supply of oxygenated water from the surface. Other effects of eutrophication can include: increased water turbidity, shifts in algal species composition (including toxic algal blooms), and changes in the species composition of benthic flora, benthic macrofauna and pelagic macrofauna (*Kemp et al.*, 2005). As an example, Chesapeake Bay has exhibited all of these environmental effects over its long history of eutrophication, particularly within the last 60 years (*Kemp et al.*, 2005). Research into the dynamics and effects of coastal ocean eutrophication is informed by a good understanding of sediment processes and their coupling to the water column.

Models of sediment dynamics have used many approaches and assumed many degrees of complexity. These different kinds of models, outlined in *Soetaert et al.* (2000), typically assume one of the following forms: (1) The simplest representations can assign constant oxygen and nutrient fluxes at the ocean bottom, or even ignore sediment fluxes altogether, and instead assign boundary-condition concentrations to the bottom waters. (2) Functional sediment models attempt to generate sediment fluxes as a function of the overlying water column state, but do not represent the sediments with any time-dependant state variables (e.g., *Middelburg et al.*, 1996; *Fennel et al.*, 2006). (3) Depth-integrated sediment models use a variety of analytical equations to designate chemical profiles within a small number of sediment layers, and the model's state variables make the sediment's behaviour history dependent (e.g., *DiToro*, 2001). (4) Depth-resolved models are usually the most complex. They divide the sediments into many layers. Some models have every layer share the same parameters (e.g., *Soetaert et al.*, 1996a), while others allow parameter values to vary between layers (e.g., *Berg et al.*, 1998).

The behaviour of any given model depends on its parameter values (i.e. specific reaction rates, diffusion rates, partitioning coefficients etc.); however, these parameters

are rarely uniform between different environments, and many cannot be measured directly. Consequently, it is common that several of these parameters are poorly quantified. Unconstrained parameters values can be estimated through tuning, i.e. fitting model output to observations by manipulating the model's parameters (*Bagniewski et al.*, 2011; *Fennel et al.*, 2001). Depending on the structure and complexity of the sediment model, this can have a number of effects. While the parameters of a complex model might easily be adapted to a particular observation set, there exists a risk of overfitting, that is, the parameters risk being fit to meaningless variation (noise) in the observations. Overfitting thus may decrease the model's ability to predict an independent set of observations. A simple model, although not as prone to overfitting, may not be able to adapt to the dynamics of the system, and thus could generate a poor fit. Parsimony is therefore the objective: to find a compromise between the sediment model's fit and complexity (*Friedrichs et al.*, 2007).

For this thesis, I have constructed a comparison of models representing complexity categories (2), (3) and (4). Evolutionary algorithms were used to tune a two-layer, depth-integrated sediment model and a multi-layer depth-resolved sediment model, representing categories (3) and (4) respectively, to observations of sediment fluxes within a mesocosm eutrophication experiment. Although both models follow a different design philosophy, they both represent the same sediment chemical processes and can be compared on this basis. Representing category (2), two functional oxygen flux models were optimized using non-linear regression and compared against the oxygen fluxes of the more complex layered models. Cross validation experiments tested to see how these models could adjust their behaviour to different environments without further tuning. These experiments were done with the intention of eventually coupling a sediment model to a regional, 3-dimensional, biogeochemical ocean model.

CHAPTER 2

METHODS

2.1 Dataset

Eutrophication experiments were performed at the Mesocosm Experimental Research Laboratory (MERL) of the University of Rhode Island between 1981 and 1983. Situated on the coast of Narragansett Bay, nine outdoor laboratory mesocosms were used to study the effects of sewage effluent on the coastal environment. Reserving three mesocosms as control, the remaining six mesocosms received inorganic nutrient inputs that varied exponentially between tanks. A full description of the experiments can be found in the MERL data reports (*Frithsen et al.*, 1985a,b,c). A brief summary of the experiments is given here.

The mesocosm tanks, 7m deep and 1.5m in diameter, were engineered to mimic the physical conditions of Narragansett Bay (Fig 3.5). Heat exchangers equilibrated the tanks with ocean water temperatures, and bay water was pumped through the tanks, effecting a turnover rate similar to that of the bay (27 days). Mesocosm sediment (40 cm deep) was transferred directly from the bay by means of a box core. Tidal mixing was simulated by an automated stirring plunger, which mixed the water column on a cycling 6 hour schedule. The mixing rates were adjusted until the mesocosm concentrations of resuspended sediment material was maintained at concentrations close to those of the bay (3 mg / L).

The six treatment tanks received nutrient inputs which increased exponentially from one tank to the next: the "1x" tank received 7.57 mM N / day, and each tank thereafter (named 2x, 4x, 8x, 16x, 32x) received double the nutrient load of the preceding tank, with

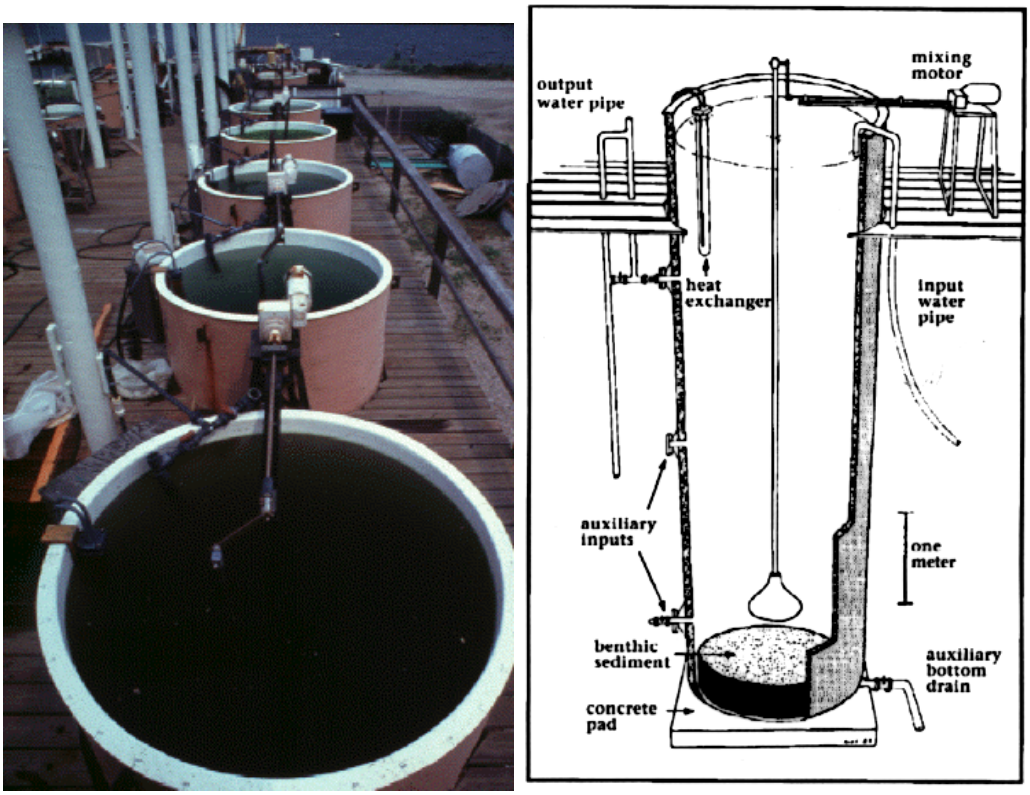

(a) Photograph (b) Schematic

Figure 2.1: The MERL Mesocosms, photos from http://www.gso.uri.edu/

the "32x" tank receiving 242.24 mM N/day. Nutrients were added in the form of inorganic salts, (NH_4Cl KH_2PO_4, $NaSiO_3 \cdot 9H_2O$) in ratios of 12.8-N : 1.0-P : 0.91-Si, matching the stoichiometry of sewage.

Throughout the two-and-a-half-year experiment, monthly measurements of water chemistry were collected, including O_2, NO_3, NH_3 and PO_4 (Fig 2.2), temperature (Fig 2.3), and salinity. Chlorophyll concentrations were estimated from observations of fluorescence, and dry weights of zooplankton were measured as well (Fig 2.4). Observations of O_2, NO_3, NH_3 and PO_4 fluxes between sediment and overlying water (Fig 2.5) were taken by covering the entire mesocosm's sediment surface with a plexiglass benthic chamber and measuring changes in nutrient and oxygen concentrations in the chamber over an hour. During the measurement, nutrient and oxygen concentrations within the chamber were modified due to reactions in the water (i.e. nitrification). To account for this, bottle samples were taken, and changes in their concentrations were measured as well. Mean flux values are listed in Table 2.1. The nutrient fluxes in many of the eutrophic mesocosms

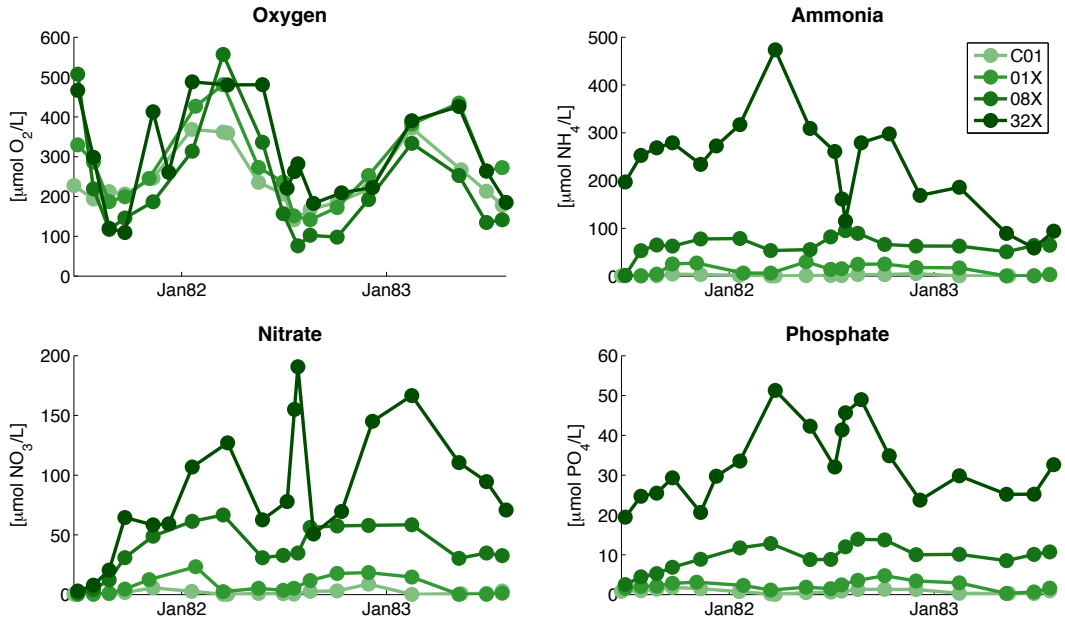

Figure 2.2: MERL water chemistry observations for four selected mesocosms

had large uncertainties (*Kelly et al.*, 1985) (Table 2.1). Nutrient fluxes in the 8X, 16X and 32X mesocosms are associated with large uncertainties, as the flux measurements required the detection of small changes in very high background concentrations. These high uncertainties were further compounded by the samples requiring dilution in order to measure the high nutrient concentrations. For this thesis, the uncertainty in the O_2 flux measurements was estimated as the standard deviation of the random error from the three control mesocosms after removing the seasonal cycle. These uncertainties were similar to those listed for a different experiment, which used the same benthic chamber measurement technique (*Oviatt et al.*, 1984). Nutrient uncertainties used within this thesis were calculated in the same manner, or taken from Kelly et al. (1985), whichever was larger. All sediment flux uncertainties used in this study are all listed in table 2.1.

Mesocosm oxygen concentrations follow a seasonal pattern of buildup due to cool temperatures and photosynthesis during the winter-spring bloom, and decrease during the heterotrophic summer season. The seasonal signal is not as strong for the nutrient concentrations; however, average concentrations roughly reflect the loading rate of their corresponding mesocosm. While chlorophyll levels appear to increase for higher loadings, oxygen levels appear to be unchanged, likely because of air-sea gas exchange of oxygen in

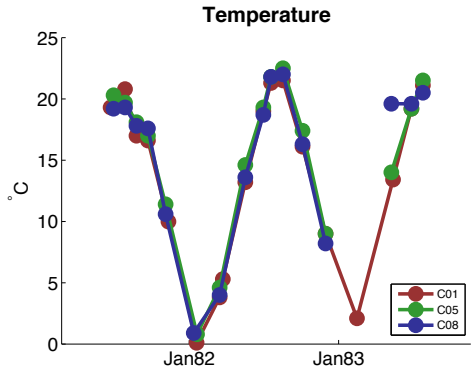

Figure 2.3: MERL temperature observations in control mesocosms

combination with daily mixing. Shortly following the chlorophyll blooms, zooplankton populations rise in response to food availability. Food competition between zooplankton and a relatively large colony of bivalves in mesocosm 8x might account for the relatively low zooplankton biomass compared to the others (*Oviatt et al.*, 1986).

For this thesis, water chemistry observations from the MERL dataset will be used as surface boundary conditions for the sediment models. Benthic flux outputs generated by the sediment models will be fit to observed fluxes. The sediment models also require inputs of a depositional flux of particulate organic matter (POM). Since the MERL dataset does not include observations of this flux, it was parameterized in a number of ways, some parameterizations requiring chlorophyll and zooplankton observations as input.

2.2 Equilibrium Model

Direct measurements of benthic reaction rates are not included in the MERL observations. For this study, rates of total carbon metabolism, denitrification, and nitrification were estimated from the observed MERL sediment fluxes by applying an equilibrium model.

The equilibrium model is based on a denitrification parameterization from *Fennel et al.* (2009), but further accounts for the conservation of nitrogen species (i.e. NO_3 and NH_4). Budgets of oxygen, ammonium, and nitrate were constructed, assuming that the sediment concentrations quickly equilibrated with the overlying water column by means of diffusion. The known fluxes from the sediments to the overlying water column are: the oxygen flux (J_{O_2}, units $\frac{\mu molO_2}{cm^2 d}$), ammonium flux ($J_{NH_4}$, units $\frac{\mu molNH_4}{cm^2 d}$) and nitrate flux

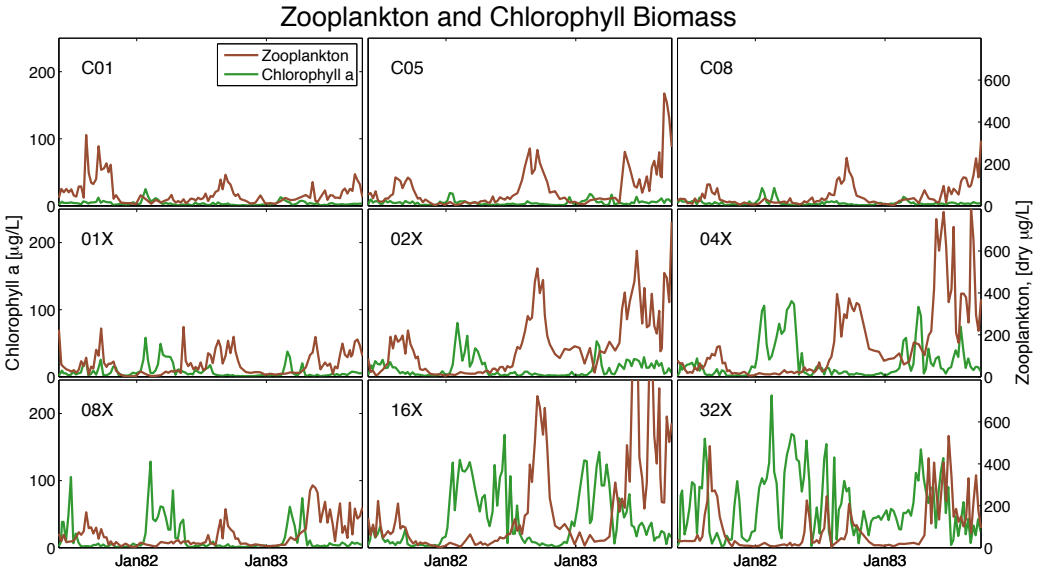

Figure 2.4: MERL chlorophyll a and zooplankton observations

(J_{NO_3}, units $\frac{\mu molNO_3}{cm^2 d}$). The four unknown, vertically integrated reaction rates are: the total rate of carbon metabolism ($R^\star_{met}$, units $\frac{\mu molC}{cm^2 d}$), the rate of carbon decomposition via the aerobic metabolism and/or the coupling of the sulphate metabolism and H_2S oxidation ($R^\star_{aer}$, units $\frac{\mu molC}{cm^2 d}$), the rate of carbon decomposition via the denitrifying metabolism ($R^\star_{dnf}$, units $\frac{\mu molC}{cm^2 d}$), and the rate of nitrification ($R^\star_{nit}$, units $\frac{\mu molO_2}{cm^2 d}$). When the Redfield ratio is assumed in designating the composition of organic matter, the following equilibrium relationships result:

$$R^\star_{met} = R^\star_{aer} + R^\star_{dnf} \tag{2.1}$$

$$J_{O_2} = -R^\star_{aer} - R^\star_{nit} \tag{2.2}$$

$$J_{NH_4} = \frac{16}{106} R^\star_{met} - \frac{1}{2} R^\star_{nit} \tag{2.3}$$

$$J_{NO_3} = \frac{1}{2} R^\star_{nit} - \frac{4}{5} R^\star_{dnf} \tag{2.4}$$

Since the fluxes of O_2, NH_4 and NO_3 are known from the MERL dataset, it is possible to

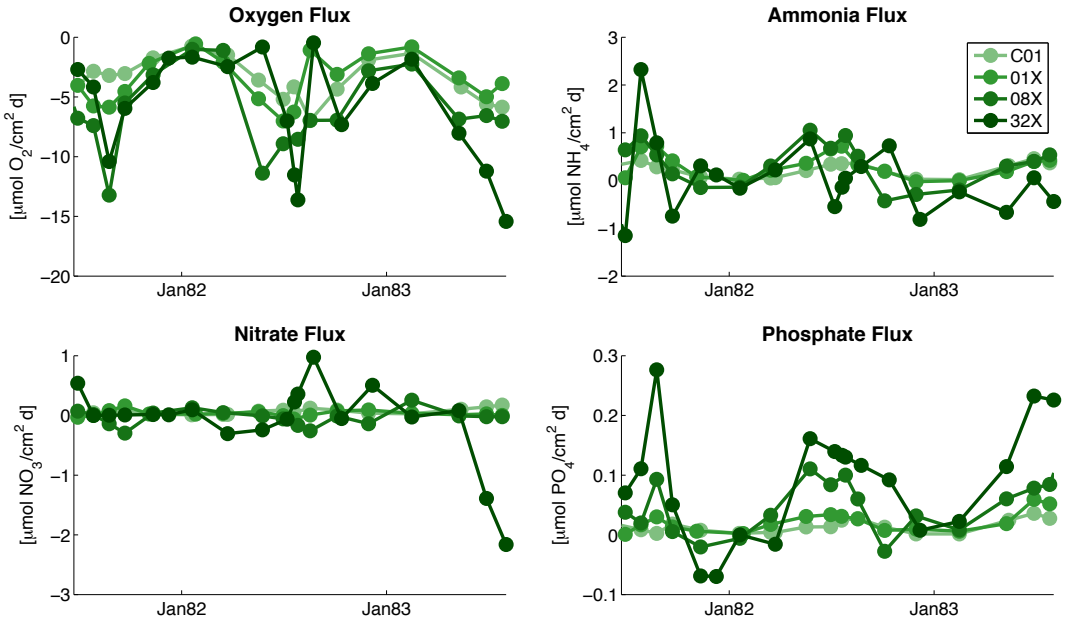

Figure 2.5: MERL benthic flux observations for four selected mesocosms

solve these four simultaneous linear equations for the four unknown reaction rates.

$$R^{\star}_{\mathrm{met}} = -(212J_{\mathrm{O_2}} - 159J_{\mathrm{NH_4}} + 265J_{\mathrm{NO_3}})/236 \quad (2.5)$$

$$R^{\star}_{\mathrm{aer}} = -(43J_{\mathrm{O_2}} - 106J_{\mathrm{NH_4}} - 20J_{\mathrm{NO_3}})/59 \quad (2.6)$$

$$R^{\star}_{\mathrm{dnf}} = -(40J_{\mathrm{O_2}} + 265J_{\mathrm{NH_4}} + 345J_{\mathrm{NO_3}})/236 \quad (2.7)$$

$$R^{\star}_{\mathrm{nit}} = -(16J_{\mathrm{O_2}} + 106J_{\mathrm{NH_4}} + 20J_{\mathrm{NO_3}})/59 \quad (2.8)$$

Within this study, reaction estimates derived in this manner will be referred to as the "equilibrium model", and they will be used for purposes to the numerical sediment models. Error estimates of the equilibrium model were assessed by propagating flux errors through these formulae.

2.3 Two-Layer Model

The two-layer sediment model (*DiToro*, 2001) examined in this study was originally designed to serve as a subroutine for the Row-Column AESOP (RCA) water column eutrophication model (*Fitzpatrick*, 2004), but now can be used as a stand-alone model.

Table 2.1: Mean MERL Benthic Fluxes

Flux	C01	C05	C08
$\bar{J}_{\mathrm{O}_2}$	-3.5±0.6	-3.3±0.6	-3.9±0.6
$\bar{J}_{\mathrm{NH}_4}$	$2.3\pm0.1\times10^{-1}$	$2.5\pm0.7\times10^{-1}$	$2.7\pm0.4\times10^{-1}$
$\bar{J}_{\mathrm{NO}_3}$	$6.4\pm3.6\times10^{-2}$	$1.8\pm3.6\times10^{-2}$	$3.7\pm3.6\times10^{-2}$
$\bar{J}_{\mathrm{PO}_4}$	$1.3\pm0.7\times10^{-2}$	$1.7\pm0.5\times10^{-2}$	$1.9\pm1.0\times10^{-2}$
-	01X	02X	04X
$\bar{J}_{\mathrm{O}_2}$	-4.7±0.6	-3.6±0.6	-4.4±0.6
$\bar{J}_{\mathrm{NH}_4}$	$4.0\pm2.2\times10^{-1}$	-3.7±0.036	1.2 ± 2.2^{-1}
$\bar{J}_{\mathrm{NO}_3}$	$4.3\pm2.4\times10^{-2}$	$3.2\pm7.2\times10^{-2}$	$12.0 \pm 2.6\times10^{-2}$
$\bar{J}_{\mathrm{PO}_4}$	$2.7\pm1.2\times10^{-2}$	$2.1\pm1.0\times10^{-2}$	$0.7\mathrm{p} \pm 1.2\times10^{-2}$
-	08X	16X	32X
$\bar{J}_{\mathrm{O}_2}$	-6.3±0.6	-5.7±0.6	-6.0±0.6
$\bar{J}_{\mathrm{NH}_4}$	$3.4\pm2.2\times10^{-1}$	$7.6\pm10.97\times10^{-1}$	$4.5\pm111.6\times10^{-2}$
$\bar{J}_{\mathrm{NO}_3}$	$-3.3\pm116.4\times10^{-2}$	$-1.1\pm23.28\times10^{-1}$	$-7.4\pm337.7\times10^{-2}$
$\bar{J}_{\mathrm{PO}_4}$	$4.4\pm12.5\times10^{-2}$	$7.6\pm8.6\times10^{-2}$	$9.1\pm5.8\times10^{-2}$

It simulates sediment chemistry and vertical transport within two vertically integrated layers, a thin aerobic layer on the surface and a large anaerobic layer below. The chemical reactions represented in the model vary between the two layers, but altogether include the decomposition of organic carbon due to a sulphate metabolism, denitrification, and methane production; nitrification, hydrogen sulfide oxidation and methane oxidation take place in the aerobic pore waters. Aerobic decomposition is not modelled. In its place, the sulphate metabolism consumes an equivalent amount of oxygen when its end product, H_2S is oxidized.

Model inputs include its state variable initial conditions, the temperature, nutrient and oxygen concentrations of the overlying-water, and the depositional flux of particulate organic matter (POM flux). Surface nutrient exchange fluxes, a sediment oxygen demand (i.e. the magnitude of the oxygen flux into the sediment), reaction rates, and chemical species distribution, are all outputs. State variables include three lability classes of particulate carbon, dissolved NO_3, and both sorbed and dissolved forms for each of NH_3, PO_4, Si, H_2S, and CH_4. All materials are budgeted with mass balance equations of the form,

$$\frac{dC_1}{dt} = R_{src,1} - R_{snk,1} + \frac{L_{\mathrm{olwc},1}\left(C_{olwc} - C_1\right) - L_{1,2}\left(C_1 - C_2\right)}{H_1} - \frac{L_{sed}(C_1)}{H_1} \quad (2.9)$$

$$\frac{dC_2}{dt} = R_{src,2} - R_{snk,2} + \frac{L_{1,2}\left(C_1 - C_2\right)}{H_2} - \frac{L_{sed}(C_2 - C_1)}{H_2}, \quad (2.10)$$

where C_{olwc}, C_1, and C_2 are a chemical's concentration in the overlying water column (units $\left[\frac{\mu\text{mol}}{\text{cm}^3}\right]$), layer 1 and layer 2 respectively, H_1 and H_2 are the layer thicknesses (units [cm]), $R_{\text{src},1}$, $R_{\text{src},2}$, $R_{\text{snk},1}$ and $R_{\text{snk},2}$ are the nutrients' chemical sources and sinks for each layer (units $\left[\frac{\mu\text{mol}}{\text{cm}^3\cdot\text{d}}\right]$), L_{sed} controls the rate of material removal from the bottom of each layer due to burial (units $\left[\frac{\text{cm}}{\text{d}}\right]$), and $L_{\text{olwc},1}$ and $L_{1,2}$ are mass-transfer coefficients (units $\frac{\text{cm}}{\text{d}}$), which describe the diffusive transports of materials (see below). Note that a mass transfer coefficient for diffusion $L_{i,j}$ can be re-written as the ratio of the diffusion rate $D_{i,j}$ (units $\left[\frac{\text{cm}^2}{\text{d}}\right]$), and layer depth, H (units [cm]).

$$L_{i,j} = \frac{D_{i,j}}{H}. \tag{2.11}$$

The diffusive transports in the mass balance equations are used to describe several processes. Bioturbation is represented within the model as a diffusive transport of solid materials between the model's two layers. Aqueous substances are transported through the sediment porewater by molecular diffusion and biological activity. All of these diffusive transports are described within the mass balance equations as a first-order Fick's second law, which states that the time derivative of a substance's concentration C is proportional to the spatial derivative of that material's flux, J:

$$\frac{\partial C}{\partial t} = -\frac{\partial J}{\partial z} \tag{2.12}$$

while according to Fick's first law, the flux J is proportional to the gradient of C,

$$J = -D\frac{\partial C}{\partial z}, \tag{2.13}$$

where D is a diffusion constant. Thus, in the two mass balance equations we find that $L_{\text{olwc},1}\,(C_{olwc} - C_1)$, $L_{1,2}\,(C_1 - C_2)$ and $L_{1,2}\,(C_1 - C_2)$ represent diffusive fluxes at the boundaries of each layer, and thus $\frac{L_{\text{olwc},1}(C_{olwc}-C_1)-L_{1,2}(C_1-C_2)}{H_1}$ and $\frac{L_{1,2}(C_1-C_2)-0}{H_2}$, are the derivatives of the flux of C across the sediment layers.

The two-layer model's algorithm can be described as follows:

1. Estimate the sediment oxygen demand, $R^{\star}_{\text{SOD}}$, $\left[\frac{\text{gO}_2}{\text{cm}^2\text{d}}\right]$, i.e. the vertically integrated rate of oxygen consumption in the sediment. Use either the value from the previous timestep, or if the simulation just started, use $R^{\star}_{\text{SOD}}$ = 0.

2. Estimate the benthic surface mass transfer coefficient ($L_{olwc,1}$, $\left[\frac{\mathrm{cm}}{\mathrm{d}}\right]$) and aerobic layer depth (H_1, $[\mathrm{cm}]$), by assuming that the diffusive influx of oxygen and sediment oxygen demand are in equilibrium, i.e.

$$R^{\star}_{\mathrm{SOD}} = D_{\mathrm{pw}}\theta_{pw}^{(T-20)}\frac{[\mathrm{O_2}]_{\mathrm{olwc}} - [\mathrm{O_2}]_2}{H_1}, \tag{2.14}$$

where D_{pw} is the diffusion rate constant for dissolved porewater substances, $\theta_{\mathrm{pw}}^{(T-20)}$, is a temperature correction factor which increases diffusion with temperature, $[\mathrm{O_2}]_{\mathrm{olwc}}$ is the overlying water column oxygen concentration, and $[\mathrm{O_2}]_2$ is the oxygen concentration at the very bottom of the aerobic layer, i.e. $[\mathrm{O_2}]_2 = 0$. Combining equations 2.11 and 2.14, we find

$$L_{olwc,1} = \frac{R^{*}_{olwc}}{[O_2]_{olwc}} \tag{2.15}$$

3. Calculate the concentration of oxygen in the upper layer. As mentioned above, the upper sediment's diffusive gradient of oxygen is approximated to drop off linearly. The oxygen concentration thus varies linearly between the concentration of the overlying water column $[\mathrm{O_2}]_{\mathrm{olwc}}$ to zero at the bottom of the aerobic layer. Integrating over across this gradient, the aerobic layer's average oxygen concentration is therefore $[\mathrm{O_2}]_1 = \frac{[\mathrm{O_2}]_{\mathrm{olwc}}}{2}$.

4. Calculate mass balance of all chemical species. Source and sink terms are calculated for the model reactions: denitrification, sulfate reduction, methane production, nitrification, sulfide oxidation and methane oxidation (Fig 2.6). Transport terms are also calculated. Surface sediment fluxes are estimated by assuming that diffusion constants are similar across all species:

$$J_{NH_4} = L_{\mathrm{olwc},1}\left([NH_4]_{olwc} - [NH_4]_1\right) \tag{2.16}$$

$$J_{NO_3} = L_{\mathrm{olwc},1}\left([NO_3]_{olwc} - [NO_3]_1\right) \tag{2.17}$$

$$J_{PO_4} = L_{\mathrm{olwc},1}\left([PO_4]_{olwc} - [PO_4]_1\right) \tag{2.18}$$

Between sediment layers, diffusion governs the vertical transport of dissolved species, and bioturbation the transport of solids (Fig. 2.7). The model's mass

balance equations are solved implicitly to find chemical species concentrations in the two layers. Because the mass balance equations include transport between the layers, the implicit solution requires solving them as two simultaneous linear equations.

Some substances react to their chemical environment by changing between solid and aqueous phases, and thus they are able to be transported via both bioturbation and porewater diffusion. For these substances their solid and aqueous partitions are calculated each timestep. To do this, the overall concentration of a chemical species C is calculated from its solid and aqueous phases, and re-partitioned such that the porewater concentration of the aqueous phase C_{pw} $\left[\frac{\mu mol}{cm^3}\right]$, and the solid concentrations of the solid phase C_s satisfy the ratio $\Pi_C = \frac{C_s}{C_{pw}}$, where Π is either a model parameter, or calculated quantity. In either case, Π is intended to function as an equilibrium constant of dissolution. The solubility of some substances is dependent on the chemistry of its environment, and thus the chemical's partition parameter Π may differ between aerobic and anaerobic layers. For example, the phosphate partitioning parameter in the aerobic layer is calculated from three model parameters, $\pi_{\mathrm{PO4,base}}$ $\left(\text{units}\frac{\text{cm}^3\text{(solid volume units)}}{\text{cm}^3\text{(porewater volume units)}}\right)$, $\pi_{\mathrm{PO4,exp}}$ (unitless), $[O_2]_{\mathrm{crit}}$ (units $\frac{\mu\mathrm{mol}}{\mathrm{cm}^3}$):

$$\Pi_{\mathrm{PO_4}} = \pi_{\mathrm{PO4,base}}\pi_{\mathrm{PO4,exp}}^{\left(\frac{[O_2]}{[O_2]_{\mathrm{crit}}}\right)}; [O_2] < [O_2]_{\mathrm{crit}} \quad (2.19)$$

$$\Pi_{\mathrm{PO_4}} = \pi_{\mathrm{PO4,base}}; [O_2] >= [O_2]_{\mathrm{crit}} \quad (2.20)$$

5. After the above calculations, the model finds a new $R^{\star}_{\mathrm{SOD}}$ from the demands of nitrification ($R^{\star}_{\mathrm{NSOD}}$) and the oxidation of sulfide and methane ($R^{\star}_{\mathrm{CSOD}}$). Note that $R^{\star}_{\mathrm{NSOD}}$ and $R^{\star}_{\mathrm{CSOD}}$ are themselves functions of the original estimate of $R^{\star}_{\mathrm{SOD}}$ from step 1.

6. Lastly, a root-finding algorithm is implemented to solve the equation

$$0 = R^{\star}_{\mathrm{NSOD}}(R^{\star}_{\mathrm{SOD}}) + R^{\star}_{\mathrm{CSOD}}(R^{\star}_{\mathrm{SOD}}) - R^{\star}_{\mathrm{SOD}}. \quad (2.21)$$

Each timestep, the algorithm iterates steps 2 through 4 until the estimate of $R^{\star}_{\mathrm{SOD}}$ converges and satisfies this equation. Once satisfied, the timestep is complete, and the next timestep begins with step 1.

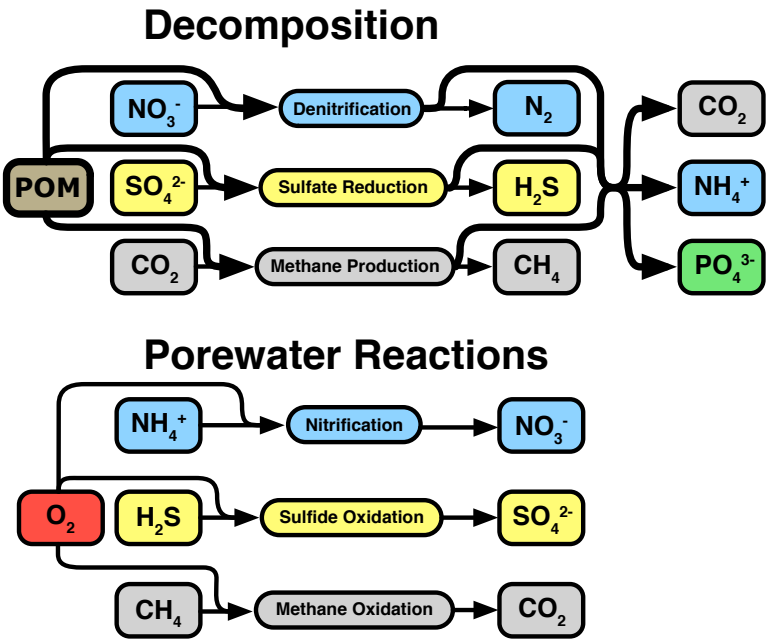

Figure 2.6: Chemical Reactions of the Two-Layer Model. Particulate organic matter is broken down by one of three metabolisms (denitrification, sulphate reduction, and methane production). Porewater reactions oxidize the reduced end products of the POM metabolism (nitrification, sulphide oxidation and methane oxidation.)

In each layer, the model estimates a carbon metabolic rate in proportion to the concentrations of three lability classes of carbon, $[\mathrm{C}]_\ell$, where the most labile class $\ell = 1$ decomposes over timescales of months, lability class $\ell = 2$ operates on timescales of years, and $\ell = 3$ is practically inert. These classes are made distinct by giving each its own specific rate constant $r_{\mathrm{met},\ell}$, which is re-scaled by an approximated Arrhenius factor $\theta_{met,\ell}^{(T-20)}$. Thus, in a given layer, the rate of carbon metabolism, R_{met} (units $\frac{\mu\mathrm{molC}}{\mathrm{cm}^3\mathrm{d}}$), is therefore:

$$R_{\mathrm{met}} = \sum_{\ell} r_{\mathrm{met},\ell}\theta_{\ell}^{(T-20)}[C]_{\ell}. \tag{2.22}$$

Next, for each layer, the rates of denitrification $R_{\mathrm{dnf},1}$, $R_{\mathrm{dnf},2}$ (units $\frac{\mu\mathrm{molC}}{\mathrm{cm}^3\mathrm{d}}$) are calculated to be proportional with the layer's NO_3 concentrations. Denitrification rates are sensitive to oxygen concentrations, and so the aerobic and anaerobic layers each have their own specific rate of reaction $r_{\mathrm{dnf},1}$ and $r_{\mathrm{dnf},2}$ (units $\frac{1}{d}$), but share an approximated

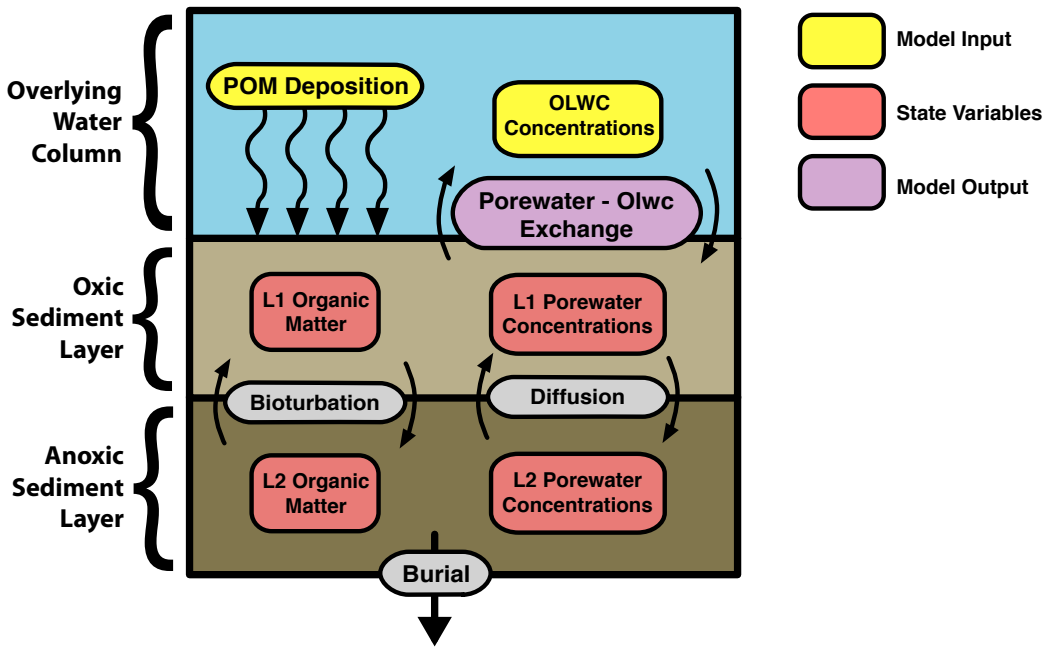

Figure 2.7: Transports of the two-layer model. Influxes of particulate organic matter fuel the carbon metabolisms. Solids are bioturbated between layers, while aqueous phases are diffused. The surface benthic fluxes are model outputs.

Arrhenius factor $\theta_{\mathrm{dnf}}^{T-20}$.

$$R_{\mathrm{dnf},1} = r_{\mathrm{dnf},1}\theta_{\mathrm{dnf}}^{(T-20)}\left[\mathrm{NO_3}\right]_1 \tag{2.23}$$

$$R_{\mathrm{dnf},2} = r_{\mathrm{dnf},2}\theta_{\mathrm{dnf}}^{(T-20)}\left[\mathrm{NO_3}\right]_2 \tag{2.24}$$

This rate, when converted to equivalent carbon units is subtracted from the total of consumed carbon. The remainder of the decomposed carbon is usually consumed by the sulphate reduction metabolism. In the rare case that [SO_4] is still too low to fuel the entire metabolic demand, methane production processes the remainder. This is done by calculating a sulphate reduction layer depth ($H_{SO_4} \leq H_2$) by linearly approximating the SO_4 diffusion gradient and finding the depth where [SO_4] reaches zero. Sulphate reduction and methane production metabolisms are then partitioned as $\frac{H_{SO_4}}{H_2}$ and $(1 - \frac{H_{SO_4}}{H_2})$ respectively.

The nitrification reaction rate R_{nit} (units $\frac{\mu\mathrm{molN}}{\mathrm{cm^3 d}}$) are proportional to the specific reaction rate r_{nit}, are proportional to $[NH_4]_1$, and are modified by an O_2 Michaelis-Menten term, and an Arrhenius factor. The rate is also modified by an NH_4 Michaelis-Menten

factor, although the half saturation parameter, $k_{\mathrm{nit,NH_4}}$ (units $\frac{\mu\mathrm{molN}}{\mathrm{cm}^3}$), is modified by its own Arrhenius factor, θ_{k,nit,NH_4}. Note that this reaction occurs only in the aerobic layer.

$$R_{\mathrm{nit}} = r_{\mathrm{nit}}\theta_{\mathrm{nit}}^{T-20}\frac{[\mathrm{NH_4}]_1}{k_{\mathrm{nit,NH_4}}\theta_{k,nit,NH_4}+[\mathrm{NH_4}]_1}\frac{[\mathrm{O_2}]_1}{k_{\mathrm{nit,O_2}}+[\mathrm{O_2}]_1}. \tag{2.25}$$

Oxidation rates of H_2S in the aerobic layer is calculated using different specific rate constants, $r_{\mathrm{H_2S},s}$ for solid phase of H_2S, and $r_{\mathrm{H_2S},pw}$ for the aqueous phase (units $\frac{1}{\mathrm{d}}$). Both phases share the same Arrhenius factor, and vary linearly with oxygen. Parameter $k_{\mathrm{H_2S,ox}}$ functions only for unit conversion.

$$R_{\mathrm{H_2S,aq}} = r_{\mathrm{H_2S,aq}}\theta_{\mathrm{H_2S}}^{T-20}\frac{[\mathrm{O_2}]_1}{k_{\mathrm{H_2Sox}}}[\mathrm{H_2S}]_{\mathrm{aq}} \tag{2.26}$$

$$R_{\mathrm{H_2S,s}} = r_{\mathrm{H_2S,s}}\theta_{\mathrm{H_2S}}^{T-20}\frac{[\mathrm{O_2}]_1}{k_{\mathrm{H_2Sox}}}[\mathrm{H_2S}]_{\mathrm{s}}. \tag{2.27}$$

The methane oxidation rates, $R_{\mathrm{CH_4ox}}$ (units $\frac{\mu\mathrm{molC}}{\mathrm{cm}^3\mathrm{d}}$), are calculated with a specific rate constant $r_{\mathrm{CH_4ox}}$ (units $\frac{1}{d}$), and Arrhenius factor $\theta_{\mathrm{CH_4ox}}^{T-20}$, a Michaelis-Menton oxygen factor $\frac{[\mathrm{O_2}]_1}{k_{\mathrm{CH_4ox}}+[\mathrm{O_2}]_1}$, and varies in proportion to methane concenrations:

$$R_{\mathrm{CH_4ox}} = r_{\mathrm{CH_4ox}}\theta_{\mathrm{CH_4ox}}^{T-20}\frac{[\mathrm{O_2}]_1}{k_{\mathrm{CH_4ox}}+[\mathrm{O_2}]_1}[\mathrm{H_2S}]_{\mathrm{aq}} \tag{2.28}$$

Bioturbation is modelled as a diffusive process, however, the two-layer model acknowledges that this transport is the result of biological activity. This is done by adjusting a base diffusion rate, D_s ($\frac{\mathrm{cm}^2}{\mathrm{d}}$), according to temperature, food availability (i.e. organic carbon in the sediment), and oxygen availability. The resulting mass transfer coefficient is

$$L'_{12,\mathrm{s}} = \frac{D_s}{H_2}\theta_{\mathrm{D_s}}^{T-20}\frac{[C]_1}{[C]_{\mathrm{ref}}}\frac{[\mathrm{O_2}]_{\mathrm{olwc}}}{[\mathrm{O_2}]_{\mathrm{olwc}}+k_{\mathrm{O_2},D_p}}, \tag{2.29}$$

where $\theta_{D_p}^{T-20}\frac{[\mathrm{O_2}]_1}{1}$ is an Arrhenius factor which varies with temperature, $\frac{[C]_1}{[C]_{\mathrm{ref}}}$ is a normalized concentration of organic carbon within the aerobic sediments, $k_{\mathrm{O_2},D_p}$ is a Michaelis-Menten half saturation constant for oxygen (units $\frac{\mu\mathrm{molO}}{\mathrm{cm}^3}$), and H_2 is the thickness of the anaerobic layer.

The two-layer model also simulates stress on benthic fauna which results from low oxygen concentrations. A model state variable, stress, S (unitless), evolves according to

the equation

$$\frac{dS}{dt} = -r_s S + \frac{k_{\mathrm{O}_2,Dp}}{k_{\mathrm{O}_2,Dp} + [\mathrm{O}_2]_{\mathrm{olwc}}} \tag{2.30}$$

where r_s (units $\frac{1}{days}$) is the specific rate of decay for stress. This equation describes stress to grow under low oxygen conditions, and dissipate when the water is well oxygenated. When the benthic community accumulates any amount of stress, bioturbation is then proportionately reduced for the remainder of the year according to the equation

$$L_{12,\mathrm{s}} = L'_{12,\mathrm{s}} \min(1 - r_s S) \tag{2.31}$$

where the function min(1 - $k_s S$) represents the annual minimum of the quantity (1 - $k_s S$).

It should be noted that the above text uses specific rate constants r (units $\frac{1}{d}$) when describing system dynamics, while the two-layer model's actual implementation usually uses reaction velocities, κ (units $\frac{cm}{d}$) which are defined as $\kappa = \sqrt{D_{\mathrm{pw}} k}$, where D_{pw} is the porewater diffusion constant. Essentially, this means that many of the above instances of a rate constant r would be substituted in the two-layer model code by $\frac{\kappa^2}{D_{\mathrm{pw}}}$. This distinction does not result in any functional difference, but only in the values of the listed parameters. A comprehensive list of two-layer model parameters are given in table A.1.

2.4 Multi-Layer Model

A multi-layer model, described by *Soetaert et al.* (1996a,b) has a vertically resolved design, dividing the sediment into multiple layers, each layer describing the same transports and chemical reactions. I have modified the multi-layer model from its original design to include phosphate so that it can be compared to the two-layer model. The state variables of the multi-layer model are O_2, NO_3, NH_3, aqueous and solid (i.e. sorbed) PO_4, two lability classes of organic carbon, and oxygen demand units ODU. The ODU variable represents reduced materials and chemicals which result from anaerobic metabolisms and are measured in concentrations of oxygen. Receiving overlying water column concentrations, depositional fluxes of organic carbon, and state variable initial conditions as input, the model computes surface fluxes, reaction rates, transport rates, and state variable concentrations. All chemical species described in the multi-layer model obey mass balance

equations, which are solved using the Euler forward method,

$$\frac{\partial C}{\partial t} = R_{src} - R_{snk} - \frac{\partial}{\partial z}\left(D\frac{\partial C}{\partial z}\right) - v_{\mathrm{sed}}\frac{\partial C}{\partial z}, \tag{2.32}$$

where C is a chemical concentration, R_{src} and R_{snk} are the chemical's sources and sinks (units $\frac{\mu\mathrm{mol}}{\mathrm{cm}^3\mathrm{d}}$), D is the Fick's law diffusion constant (units $\frac{\mathrm{cm}^2}{\mathrm{d}}$), and v_{sed} is the burial speed (units $\frac{\mathrm{cm}}{\mathrm{d}}$), which results from a slowly rising coordinate system that is compensating for the constant addition of sediment materials at the sediment surface (defined as $z = 0$). Diffusion transports aqueous material between layers, while bioturbation transports solids. Figure 2.9 summarizes the model's modes of physical transport. As in the two-layer model, phosphate can be converted between solid and aqueous phases. Chemical reactions include aerobic decomposition, denitrification, anaerobic decomposition (which produces ODUs), the oxidation of ammonium, and the oxidation of ODUs (Fig 2.8). Rates of the oxidation reactions are calculated using a specific rate constant (r) and Michaelis-Menten half saturation constants (k). For nitrification:

$$R_{\mathrm{nit}} = r_{\mathrm{nit}}[\mathrm{NH_4}]\frac{[\mathrm{O_2}]}{\mathrm{O_2} + k_{O_2,\mathrm{nit}}} \tag{2.33}$$

For ODU oxidation:

$$R_{\mathrm{ODUox}} = r_{\mathrm{ODUox}}[\mathrm{ODU}]\frac{\mathrm{O_2}}{[\mathrm{O_2}] + k_{\mathrm{ODUox},O_2}} \tag{2.34}$$

Computation of the reaction rates for the three metabolisms first estimates the total decomposed carbon, and then partitions the decomposition between the three metabolisms depending on the availability of oxygen and nitrate. The rate of carbon decomposition in a given layer is:

$$R_{met} = \sum_{\ell=1}^{2} r_{\mathrm{met}_\ell}[C]_\ell \theta_{\mathrm{met}_\ell}^{(T-20)} \tag{2.35}$$

where r_{met_ℓ} is the specific rate constant for carbon lability class $\ell = 1, 2$, and θ_{met_ℓ} is an Arrhenius factor. Three limitation terms are then calculated, (lim_{aer}, lim_{dnf}, and

lim_{anox}) and summed ($\sum lim$).

$$lim_{\text{aer}} = \frac{[O_2]}{[O_2] + k_{\text{aer},O_2}} \tag{2.36}$$

$$lim_{\text{dnf}} = \frac{[NO_3]}{[NO_3] + k_{\text{dnf},NO_3}} \frac{k_{\text{dnf},O_2}}{[O_2] + k_{\text{dnf},O_2}} \tag{2.37}$$

$$lim_{\text{anox}} = \frac{k_{\text{anox},NO_3}}{[NO_3] + k_{\text{anox},NO_3}} \frac{k_{\text{anox},O_2}}{[O_2] + k_{\text{anox},O_2}} \tag{2.38}$$

$$\sum lim = lim_{\text{aer}} + lim_{\text{dnf}} + lim_{\text{anox}} \tag{2.39}$$

The model then assigns the fraction of decomposed carbon to each metabolism as $\mathrm{R}_{\text{met}} \frac{lim_{\text{aer}}}{\sum lim}$, $\mathrm{R}_{\text{met}} \frac{lim_{\text{dnf}}}{\sum lim}$, $\mathrm{R}_{\text{met}} \frac{lim_{\text{anox}}}{\sum lim}$ to aerobic decomposition, denitrification and anaerobic decomposition, respectively.

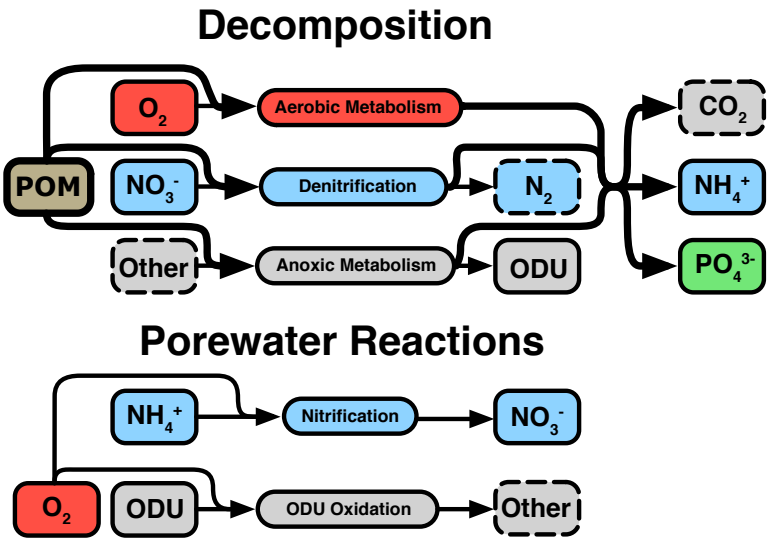

Figure 2.8: Chemical reactions of the multi-layer model. Particulate organic matter is decomposed by one of three metabolisms (aerobic, denitrification or anaerobic). Porewater reactions (nitrification, ODU redox) oxidize the reduced end products of the three metabolisms.

2.5 POM Flux Parametrizations

Both the multi- and two-layer models require a depositional flux of particulate organic matter (POM) as input. These fluxes were not measured during the MERL eutrophication

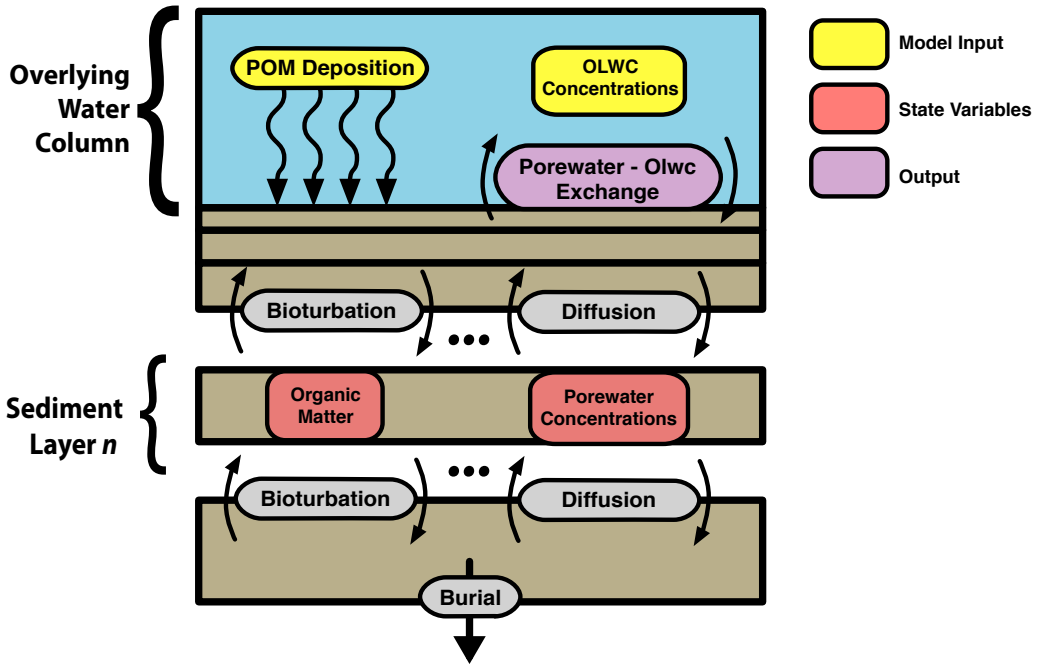

Figure 2.9: Transport processes of the multi-layer model. The surface layer receives an influx of particulate organic matter. Solids are transported between layers via bioturbation. Aqueous phases are transported between layers via diffusion. The benthic oxygen and nutrient fluxes are the model output.

experiments, and had to parameterized. Four parameterization methods were optimized in a number of ways. "Joint" parameterizations fit POM flux parameters using data from all of the mesocosms, while "individual" parameterizations constrain a different flux parameter value for each mesocosm. In additional trials, sediment model parameters were included in the optimization. These trials used both the two-layer and multi-layer model. Parameterizations of POM flux were constructed as follows:

Method A: For each mesocosm, a constant POM flux rate was assigned over the entire 2.5 year simulation.

$$J_{POM} = p_{const} \tag{2.40}$$

This basic method is similar to that described in *DiToro* (2001). Note that this method was only optimized individually. In other words, the mesocosms never shared the same

constant POM flux value.

Method B: POM deposition scales in direct proportion to chlorophyll concentrations, C, i.e.,

$$J_{POM} = p_{chla}[\mathrm{Chl}]. \tag{2.41}$$

Method C: POM flux scales linearly to chlorophyll a of two phytoplankton groups: "diatom" and "other". Measured chlorophyll-a, C, is partitioned between diatoms, and other phytoplankton, using the observed abundances of diatoms, A_{dia}, and total abundance of algae, A_{tot}.

$$J_{POM} = \frac{(p_{dia}A_{dia} + p_{other}(A_{tot} - A_{dia}))}{A_{tot}}[\mathrm{Chl}]. \tag{2.42}$$

This parameterization is a generalization of method "B" and can reproduce its output by setting $p_{dia} = p_{other}$.

Method D: POM flux constructed from a linear combination of chlorophyll-a, [Chl], and zooplankton biomass, [Zoo]:

$$J_{POM} = (p_{chla}[\mathrm{C}] + p_{zoo}[\mathrm{Zoo}])\,. \tag{2.43}$$

This parameterization is also a generalization of method "B" and can reproduce its output by setting $p_{zoo} = 0$.

2.6 Simple Oxygen Flux Parameterizations

Oxygen flux parameterizations do not have state variables, but instead immediately convert an input (i.e. temperature or overlying water oxygen) into an output according to a function. For sake of comparison, the performance of two parameterizations of oxygen flux will be assessed. These models use only 1 to 2 parameters (p_1 and p_2), and accept only one or two fields as input. As a result, they are easier to implement and require negligible computational resources when compared to the two- and multi-layer models.

The first parameterization, previously suggested by *Murrell and Lehrter* (2010), describes the flux to increase linearly with oxygen supply. Is an empirical parameterization relating the benthic oxygen flux $J_{\mathrm{O_2,ML}}$ (negative sign implies a flux into the sediment), to oxygen concentration in the overlying water, O_2:

$$J_{\mathrm{O_2,ML}} = -p_1 O_2. \tag{2.44}$$

While *Murrell and Lehrter* (2010) used a second y-intercept parameter, we chose to set it to zero so that the model produces meaningful output in the limit as O_2 approches zero.

The second parameterization, used in *Hetland and DiMarco* (2008), also uses overlying water oxygen as input, but rescales the flux according to temperature by including an (approximated) Arrhenius factor. The inclusion of this factor accounts for the dependence of the sediment's metabolic rate with temperature. Inputs for this parameteriztion are therefore oxygen, O_2, and temperature, T:

$$J_{\mathrm{O_2,HD}} = -p_1 2^{\frac{T}{10}} \left(1 - e^{\left(\frac{p_2}{\mathrm{O_2}}\right)}\right). \tag{2.45}$$

Here, the $2^{\frac{T}{10}}$ allows the flux to obey a "Q_{10}" rule: that an increase in 10 degrees roughly doubles most rates of reaction. The $\left(1 - e^{\left(\frac{p_2}{\mathrm{O_2}}\right)}\right)$ factor approaches zero at low oxygen.

For the sake of brevity the *Murrell and Lehrter* (2010) parameterization will from now on be referred to as "ML10", and the *Hetland and DiMarco* (2008) will be called "HD08".

2.7 Optimization Methods

While some of the sediment model's parameters may be known prior to a simulation, it is rare that the model's entire parameter set is well quantified from the outset. Many of these parameters are difficult or impossible to measure empirically, so unknown parameters are determined in the process of optimization. During this process, a model's parameters, $\vec{p}$, are objectively constrained by methodically adjusting their values in an attempt to minimize the misfit between model output, $X_i^{mod}(\vec{p})$, and corresponding observation, X_i^{obs}.

The model-data misfit is quantified with a cost function, $F(\vec{p})$,

$$F(\vec{p}) \quad = \quad \sum_{m=1}^{M} \frac{1}{W_m} \sum_{i=1}^{I_m} \left(X_{m,i}^{obs} - X_{m,i}^{mod}(\vec{p}) \right)^2 \tag{2.46}$$

which can be algorithmically minimized by using a number of different techniques. In this definition, M is the number of different data types $m \epsilon \{J_{\mathrm{O}_2}, J_{\mathrm{NO}_3}, J_{\mathrm{NH}_4}, J_{\mathrm{PO}_4}\}$, which each have I_m observations, and are given weights W_m. The value of a data type's weighting factor was chosen to be equal to the same data type's unweighted cost contribution prior to optimization. This choice of weights normalized the unoptimized cost contribution of each data type to the value of 1.0, and prevented the cost from arbitrarily varying with the choice of units for a given data type. The exact values used in this study are W_{O_2} = 901.49 $[\frac{\mathrm{cm}^2\mathrm{d}}{\mu\mathrm{molO}_2}]^2$, W_{NO_3} = 33.37 $[\frac{\mathrm{cm}^2\mathrm{d}}{\mu\mathrm{molNO}_3}]^2$, W_{NH_4} = 29.93 $[\frac{\mathrm{cm}^2\mathrm{d}}{\mu\mathrm{molNH}_4}]^2$, and W_{PO_4} = 0.8046 $[\frac{\mathrm{cm}^2\mathrm{d}}{\mu\mathrm{molPO}_4}]^2$.

The cost function will be used to compare the model performance for a number of sediment models; however, there is uncertainty associated with the observations used to calculate the cost. The cost function, therefore, has its own bounds of uncertainty, which can be estimated by propagating observational errors (table 2.1) into the cost function calculation using a Monte Carlo method (*Bagniewski et al.*, 2011).

Three different minimization algorithms were used in this study: least squares regression, a gradient descent scheme, and an evolutionary algorithm. The latter two are described below.

Optimization of the POM flux parameterizations fitted modelled sediment fluxes to observed fluxes by algorithmically varying the POM flux parameters. The fitting algorithm used a gradient descent scheme. This algorithm starts its search of the parameter space from an initial point, numerically estimates the cost function gradient, $\frac{\partial F(\vec{p})}{\partial p_i}$, at this point and uses the gradient to estimate a new point in parameter space, i.e. a new parameter set expected to correspond to a lower cost. When the chosen parameter set is sufficiently near a cost function minimum, the gradient becomes very small, and the procedure terminates. When calculating the cost function gradient numerically, this method is used best with relatively few parameters, because estimation of the cost gradient requires one model simulation for every parameter involved, and so the required computation resources increase linearly with the number of parameters. This kind of optimization is

also deterministic and is therefore repeatable, given the same initial conditions.

The two- and multi-layer sediment models involved far more parameters than the POM flux parameterizations, making the gradient descent method computationally expensive. Evolutionary algorithms, whose required computational resources do not increase with the number of parameters, were used for these models (Fig 2.11). Evolutionary algorithms, so named due to their semblance to the mechanisms of natural selection, work as follows:

1. Initialization: A baseline parameter set $\vec{p}_{init}$ is copied n times to form a parameter set population. Diversity in the population is generated by adding noise to the copies.

2. Selection: The cost function is evaluated for each population member, and the members are sorted by cost. Members with lower cost are kept, and the remaining fraction of the population is deleted (we deleted half the members each generation).

3. Repopulation and Recombination: Those population members which remain are randomly grouped into pairs of ”parents”. From each pair of parents, a random combination of parameter values are used to generate an “offspring”, a new population member. This is repeated until the population size is replenished.

4. Mutation: The selection step requires population diversity in order to function. This diversity is maintained by applying mutations to offspring. In this manner, new parameter values may enter the population.

5. Iterate over the previous three steps for a set number of generations. For purposes of this study, thirty generations was sufficient to allow the cost function to converge to a minimum.

Note that when optimizing non-linear models, such as the two- and multi-layer sediment models, multiple local minima can exist in addition to a global minimum (Fig 2.10). Both gradient descent methods and evolutionary algorithms (with sufficiently small mutation rates) can become ”trapped” in a local minimum, and it is not easy to verify any minimum to be global. At best, comparison of repeated optimizations can test the consistency of optimizations.

Due to the simple nature of the SOD parameterizations, their parameters were easily fit to observations using a least-squares regression routine.

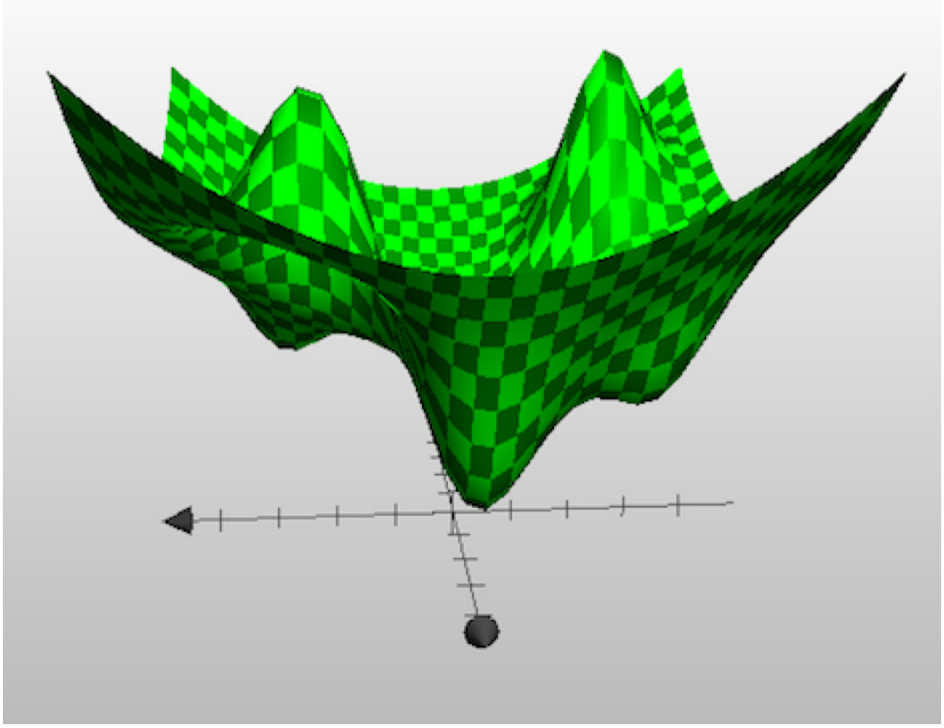

Figure 2.10: Example of an idealized cost function in 2D parameter-space, with one global and many local minima

2.8 Evaluation of Model Parsimony, the f-Test

Any phenomenon can be described to an arbitrary precision, given a sufficiently complex model. Since inaccurate models are not useful, and exceedingly complex models are impractical, success in modelling therefore lies within the compromise of the model-data fit and model's complexity. Quantitative evaluation of this compromise is possible by means of an f-test. This test compares two models, rewards them for better model-data fits, and punishing them for utilizing a larger number of parameters (i.e. for being more complex). Examples of its use in sediment modelling can be found in *Soetaert et al.* (1996c); *Berg et al.* (1998), and the procedure will be be summarized here.

The f-test uses the null hypothesis that a complex model does not significantly improve the model-data fit over that of a simpler model. If the null hypothesis is true, the value $f_{\text{test}} = \left(\frac{F_C - F_S}{(d_C - d_S)}\right) / \left(\frac{F_C}{d_C}\right)$ follows an f-distribution with ($d_S - d_C$,d_C) degrees of freedom, where F_C and F_S are the cost functions (eqn. 2.46) of the complex and simple models respectively, and d_C and d_S are their degrees of freedom (i.e. number of observations - number of model parameters - 1). If the null hypothesis is true, then the

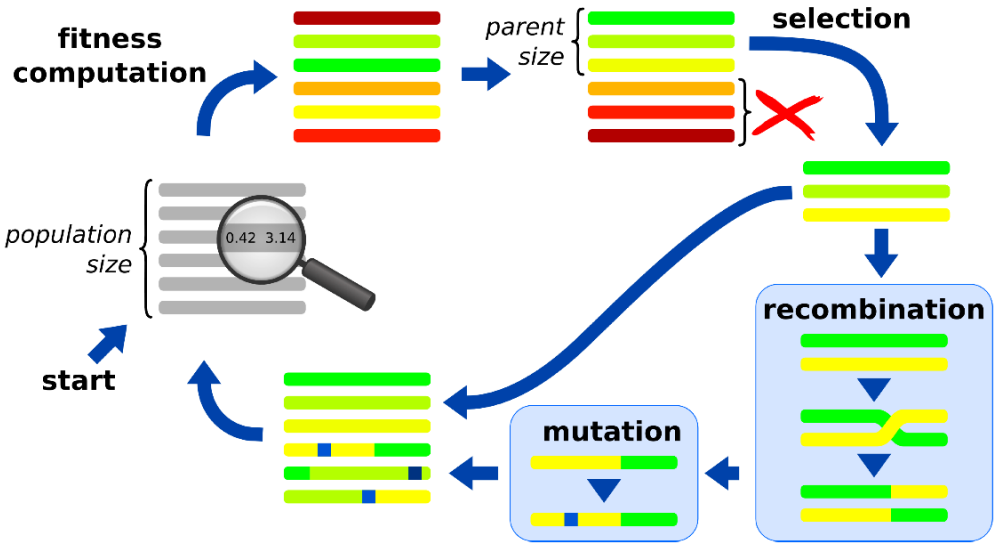

Figure 2.11: Diagram of an evolutionary algorithm. From *Mattern* (2008)

calculated value of f_{test} should be less than f-distribution's critical value (which varies with the chosen confidence interval). Thus, if f_{test} exceeds the critical value, the data is better described by the more complex model, in spite of it's larger number of parameters.

2.9 Hessian Analysis

A Hessian matrix can be defined as the matrix with elements:

$$H_{ij} = \frac{\partial^2 F(\vec{p})}{\partial p_i \partial p_j}, \tag{2.47}$$

where $F(\vec{p})$ is a model's cost function (defined in the previous section), and $\vec{p}$ is the model parameter set. When used with linear models, inverting the Hessian matrix results in the covariance matrix of the model parameters. Because the two-layer and multi-layer models are both non-linear, this process only provides an approximation of the covariance matrix, and the covariance values do not maintain a uniform value throughout parameter space. A full description of this technique may be found in *Thacker* (1989). The covariance matrix can be used to identify parameters with a large variance, as well as correlated parameters. These parameters are to be removed from the optimization process because large parameter variances indicate insensitive parameters that are difficult to constrain, and large parameter covariances indicates undesirable redundancy between the function of two parameters. By

removing these parameters, the optimization's repeatability is improved.

2.10 Cross Validation

While the process of optimization allows a model's performance to improve within a given dataset, there is reason for concern that the model's parameter set becomes over-fitted, that is, too specialized to function properly within other environments. After optimizing a model within a given dataset, it is prudent to test the model within other environments without re-tuning its parameters. Although this study has been restricted only to the MERL eutrophication dataset, a wide range of eutrophication conditions exists between mesocosms. Cross validation was accomplished by subsampling 5 of the 9 available tanks. A single list of ten random mesocosm subsets was generated, and both models were optimized using each subset. The resulting optimized models were then run in all 9 mesocosms, and the ten resulting cost functions were averaged. Because the POM flux parameterization used a different parameter for each mesocosm, it was impossible to involve them in the cross validation process, and previously optimized values were used.

CHAPTER 3

RESULTS

3.1 Hessian Analysis

As stated in chapter 2, insensitive parameters were the first to be removed from the Hessian matrix. In order to gauge their relative sensitivity, the parameter values were normalized, and the second derivatives of the cost function with respect to each parameter (i.e. the diagonal elements of H) were compared. The twelve least sensitive parameters were removed from the Hessian matrix for both models. If the second derivative with respect to a given parameter was smaller than a chosen threshold, that parameter was removed from the Hessian matrix. Without the removal of these insensitive parameters, the multi-layer model's Hessian matrix inverted into an unreasonable covariance matrix (i.e. some parameters had negative variance values).

Correlated parameters were removed next. The covariance matrices were normalized to acquire correlation matrices, which are visualized in figure 3.1. Correlated and anticorrelated parameters appear as red and blue respectively, while uncorrelated parameters appear as grey. For both models, the rows and columns of the most correlated parameters were removed until no two parameters shared a correlation higher than a chosen threshold of 0.6. Correlation matrices generated after the removal of correlated parameters are visualized in figure 3.2.

It was often required to choose between two or more correlated parameters for removal. In these cases, the choice was made with two goals in mind: first, to remove as few parameters as possible, and second, to preserve the functional diversity of the parameter set as best as possible. Tables A.1 and A.2 list all the parameters involved in the

process, and list the results of the Hessian analysis. Parameters were either "Kept" and included in the process of optimization, or they were removed either as "Insensitive" or "Correlated" parameters. Overall, 22 of the 48 two-layer model parameters were included in optimization, while 15 of the 33 multi-layer model parameters were included (see tables A.1 and A.2).

The two-layer model's parameters $r_{\mathrm{met,3}}$, $\theta_{\mathrm{met,3}}$, $\kappa_{\mathrm{H_2Sox,aq}}$, $\kappa_{\mathrm{H_2Sox,s}}$, $\pi_{\mathrm{H_2S,1}}$, $\pi_{H_2S,2}$, $\theta_{\mathrm{H_2Sox}}$, $k_{\mathrm{H_2Sox,O_2}}$, $\kappa_{\mathrm{CH_4ox}}$, $\theta_{\mathrm{CH_4ox}}$, $k_{\mathrm{CH_4ox,O_2}}$, and $k_{\mathrm{sul,SO_4}}$ were found to be insensitive and were eliminated. This result was reasonable: parameters $r_{\mathrm{met,3}}$, and $\theta_{\mathrm{met,3}}$ decompose the most inert class of organic matter over timescales which are irrelevant to the MERL mesocosm experiments; $\kappa_{\mathrm{H_2Sox,aq}}$, $\kappa_{\mathrm{H_2S,s}}$, $\pi_{\mathrm{H_2S,1}}$, $\theta_{\mathrm{H_2Sox}}$, and $k_{\mathrm{H_2Sox,O_2}}$, $k_{\mathrm{sul,SO_4}}$, directly or indirectly, govern the oxidation rate of H_2S, which is irrelevant since the model converts outfluxes of H_2S into a sediment oxygen demand; $\kappa_{\mathrm{CH_4ox}}$, $\theta_{\mathrm{CH_4ox}}$, and $k_{\mathrm{CH_4ox,O_2}}$ govern the methane production metabolism rates, which are very small in the MERL dataset and are only large on rare occasion when sulphate is depleted from the sediment.

Parameters L_{sed}, $r_{met,2}$ and $\theta_{met,2}$ were removed as they were correlated with the POM deposition parameters (i.e. p_{const}C01, p_{const}C05, and p_{const}C08). Although v_{sed} does not register as being above the .6 correlation threshold in figure 3.1(a), removal of parameters such as $r_{met,2}$ affected future iterations of the correlation matrix, and v_{sed}'s correlations grew larger. Many parameters involved with transfer and storage of aqueous and solid phosphate registered as correlated, including D_{pw}, D_{s}, $\pi_{\mathrm{PO4,base}}$, $\pi_{\mathrm{PO4,exp}}$, $r_{\mathrm{met,1}}$ and $\theta_{\mathrm{met,1}}$. From this list, $\pi_{PO_4,exp}$ was kept to preserve the functioning of the sediment phosphate storage. Many nitrification parameters were correlated, including κ_{nit}, θ_{nit}, $k_{\mathrm{nit,NH_4}}$ and $\theta_{\mathrm{k,nit,NH_4}}$. Similarly, denitrification parameters were correlated as well, including $\kappa_{\mathrm{dnf,1}}$, $r_{\mathrm{dnf,2}}$, and θ_{dnf}. In both situations, only the reaction velocities κ_{nit} and $\kappa_{\mathrm{dnf,1}}$ were kept.

Most of the multi-layer model's chemistry parameters were removed as they were found to be insensitive, including $k_{\mathrm{aer,O_2}}$, $k_{\mathrm{ODUox,O_2}}$, $k_{\mathrm{anox,ODU}}$, $k_{\mathrm{nit,O_2}}$, $k_{\mathrm{dnf,NO_3}}$, $k_{\mathrm{dnf,O_2}}$, and $k_{\mathrm{anox,NO_3}}$. Since the MERL mesocosms were consistently well-oxygenated, the oxygen saturation and inhibition parameters were not necessary for the model's proper functioning and would only have affected the model's behaviour under extremely high or low oxygen concentrations. Many of these parameters are furthermore used to weight partitions of the carbon metabolism between aerobic, denitrification and anaerobic pathways, depending on the availability of oxygen, and nitrate. There never arose any situation where oxygen

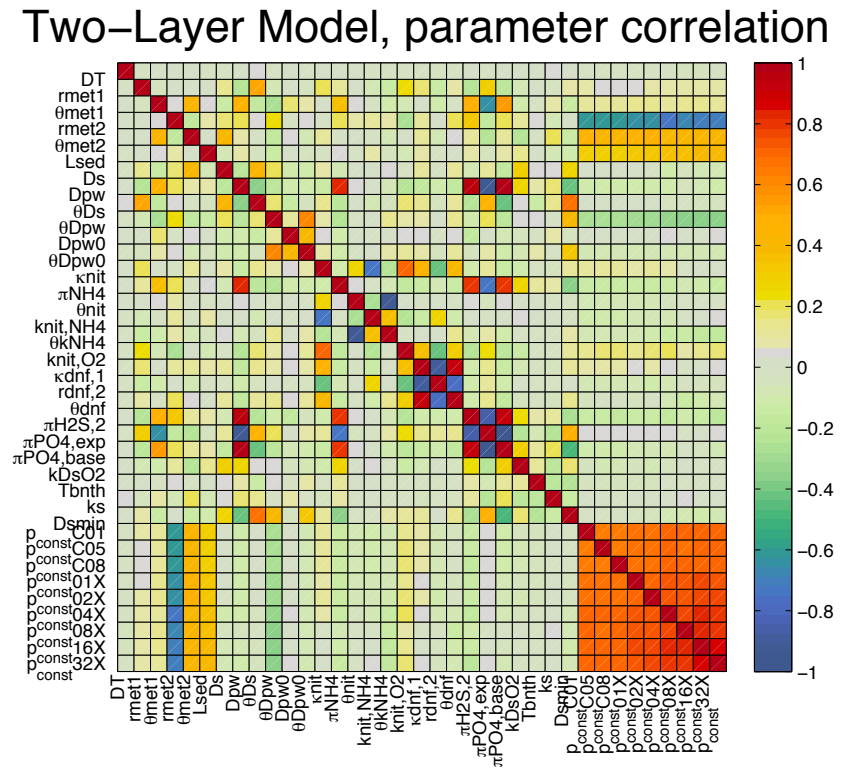

(a)

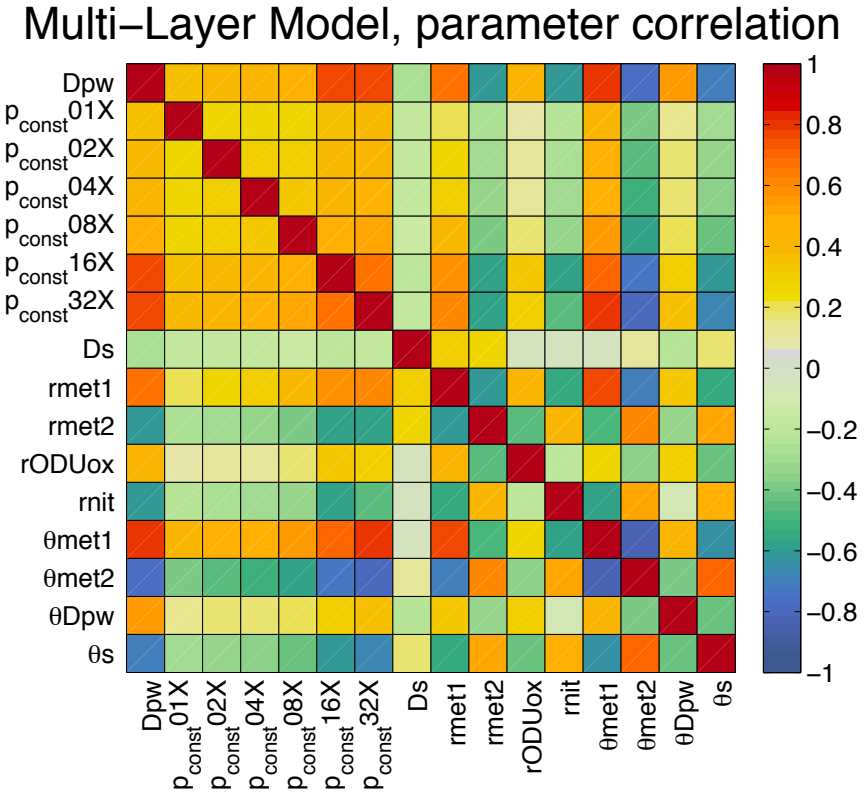

(b)

Figure 3.1: Parameter covariance for two-layer model (left) and multi-layer model (right)

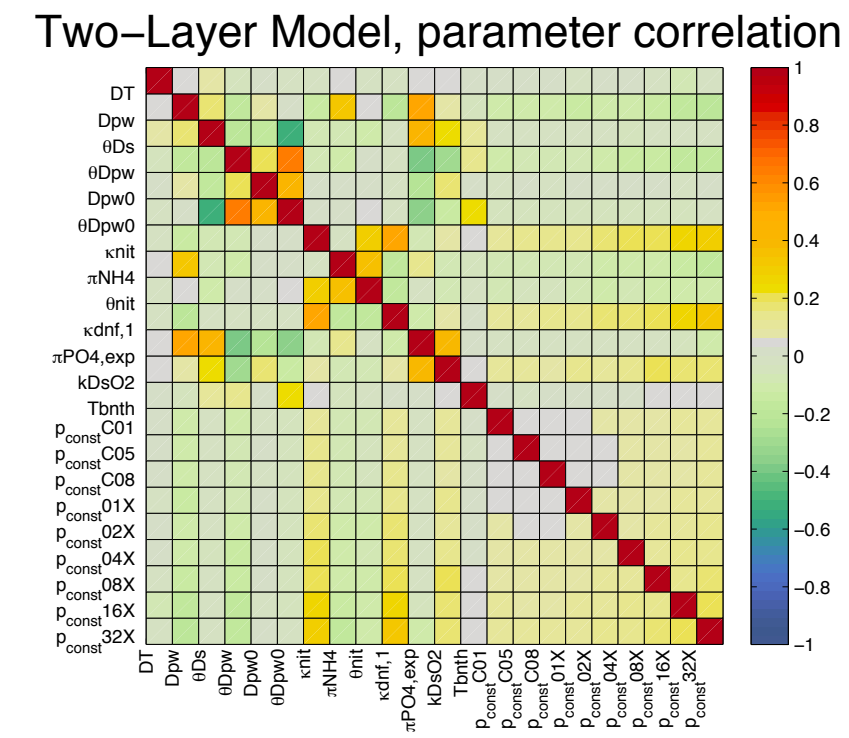

(a)

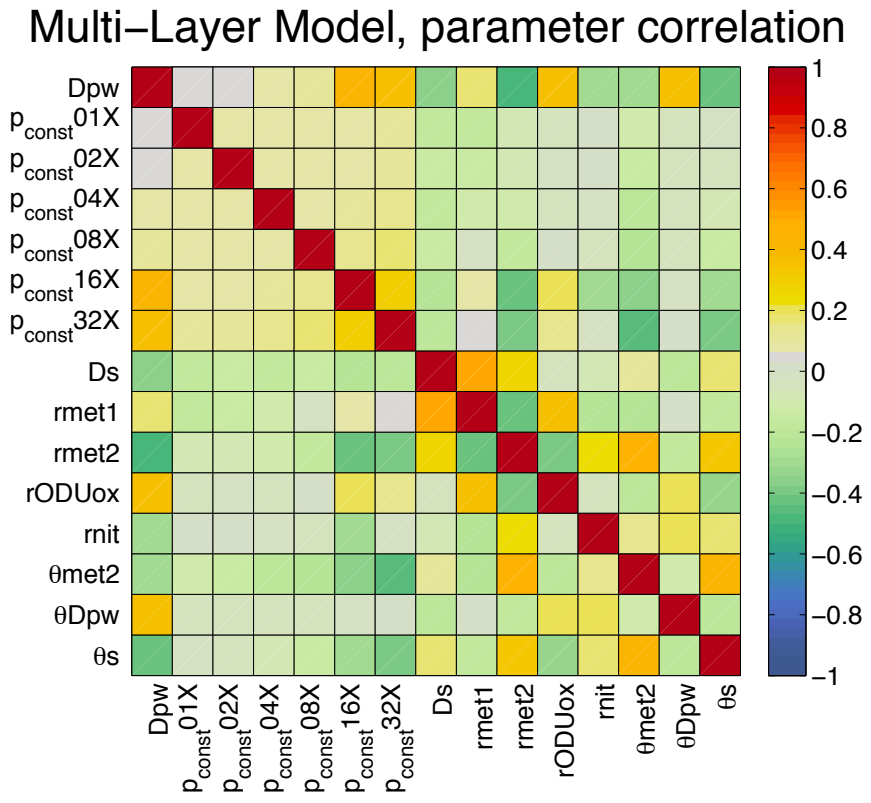

(b)

Figure 3.2: Parameter covariance for two-layer model (left) and multi-layer model (right) after the removal of correlated parameters.

concentrations dropped to sufficiently low levels that the weighting of these parameters became significant. Parameters of the anammox pathway all registered as insensitive, likely due to the fact that these reactions were inhibited by the presence of oxygen. A number of the POM depositional flux parameters (i.e. p_{const}C01, ... etc.) were among the 12 least sensitive and were removed. Since optimization of the POM parameters was necessary, these parameters were kept in spite of their removal during the Hessian analysis. Since the inverted Hessian matrix only approximates the model's covariance matrix, one cannot expect it to identify insensitive parameters with perfect accuracy.

Once the Hessian matrix was inverted however, it was straight-forward to remove correlated parameters. When $\theta_{met,1}$ was removed from the matrix, all correlations dropped below the .6 threshold.

3.2 Depositional Flux Optimizations

The depositional flux of particulate organic matter (POM) is a necessary input to the two-layer and multi-layer sediment models, but the MERL eutrophication experiment data did not include such observations. These unknown fluxes were thus parameterized and optimized for the two-layer model. Four flux parameterization methods were used: assigning a different constant POM flux to each mesocosm (method "A"); a POM flux scaled to chlorophyll concentrations in the overlying water (method "B"); a POM flux scaled to a linear combination of diatom chlorophyll and other chlorophyll (method "C"); and a POM flux scaled to a linear combination of chlorophyll and zooplankton concentrations (method "D"). The optimized cost function values for the four methods are listed in table 3.1. For methods B, C, and D, these results include "individual" parameterizations (subscript "i"), where a unique POM flux parameter was assigned to each mesocosm, and "joint" parameterizations (subscript "j"), where the same parameter was applied across all mesocosms. Uncertainties of the cost function were estimated by propagating observational errors listed in table 2.1.

Due to the exceedingly large uncertainties in the observed nutrient fluxes of the 8X, 16X and 32X mesocosms, the cost functions also had large uncertainties, too large to reliably compare the optimized cost functions. However, when the cost function was calculated from these same results, but excluding the cost contributions of mesocosms 8X, 16X and 32X, the uncertainty was sufficiently small to resolve differences in the

Table 3.1: Two-layer model: cost for all mesocosms

Flux Parameterization	**A**, flux is constant	**B**, flux scales with chl.	**C**, flux scales with diatom and other chl.	**D**, flux scales with chl. and zoop.
Individual: unique parameters for each mesocosm	3.76 ± 2.85	4.24 ± 2.85	4.12 ± 2.85	4.15 ± 2.85
Joint: shared parameters across all mesocosms	N/A	5.60 ± 2.85	5.38 ± 2.85	5.20 ± 2.85

Table 3.2: Two-layer model: cost, excluding 08X, 16X and 32X

Flux Parameterization	**A**, flux is constant	**B**, flux scales with chl.	**C**, flux scales with diatom and other chl.	**D**, flux scales with chl. and zoop.
Individual: unique parameters for each mesocosm	$0.46 \pm .04$	$0.62 \pm .05$	$0.52 \pm .05$	$0.58 \pm .04$
Joint: shared parameters across all mesocosms	N/A	$1.35 \pm .05$	$1.29 \pm .04$	$1.09 \pm .04$

costs. However, because the joint parameterizations were fit to observations from all of the mesocosms (including the noisy eutrophic mesocosms), the optimized values of the joint parameterizations were therefore overestimated.

Once the cost contributions of 8X, 16X, and 32X were excluded, comparison of the parameterization costs revealed that methods A and C_i produced the lowest misfit, their difference in costs being within the bounds of uncertainty. This means that the two-layer model output more closely resembled observations, while using one of two parameterizations: one which assigns the POM fluxes to constant values, and one that scaled nine POM fluxes with estimates of diatom chlorophyll. All other parameterizations that scaled the POM flux with other measures of pelagic biomass did not generate as good a fit.

Although method A and C_i frequently had a better fit than the other models, they were more complex (i.e. used more parameters) than the joint B, C and D methods. There remains the possibility that method A's and C_i's superior fit was a result of over-fitting, and that the simpler models were to be preferred. More generally stated, the objective

of the parameterizations was not necessarily to produce the best fit, but to find the most parsimonious one. The relative parsimony of method A and C_i against the simpler methods was tested; an f-test can check to see if a more complex model's additional parameters are justified by its increase in fit. An f-value, calculated from the cost value and number of parameters for each model, is compared against a critical value of a corresponding f-distribution. An f-value which exceeds the critical value indicates that the complex model's extra parameters were justified by the model's improved fit.

This test was performed, using cost functions that excluded contributions from mesocosms 8X, 16X and 32X. The results of these f-tests are shown in table 3.3 and table 3.4. Both methods A and C_i consistently scored an f-value that was much larger than their critical values, indicating that their extra parameters produced a statistically significant improvement in the model-data fit. Thus, on the basis of the model-data misfits (Tables 3.1, 3.2) and the f-tests (Table 3.3, 3.4) methods A and C_i were to be preferred over the other parameterizations.

Table 3.3: f-Scores and Critical Values of Two-Layer Model Input Parameterizations: Method A vs Each of Joint Methods B, C, and D

Compare **A** against:	$\mathbf{B}_j$, flux scales with chl.	$\mathbf{C}_j$, flux scales with diatom and other chl.	$\mathbf{D}_j$, flux scales with chl. and zoop.
f score	1155	1092	911
Critical Value	1.96	2.03	2.03

Table 3.4: f-test, of Two-Layer Model Inputs: Method C_i vs joint Methods B, C, and D

Compare **A** against:	$\mathbf{B}_j$, flux scales with chl.	$\mathbf{C}_j$, flux scales with diatom and other chl.	$\mathbf{D}_j$, flux scales with chl. and zoop.
f score	1033	982	824
Critical Value	1.65	1.67	1.67

The resulting overall mean POM fluxes are plotted in figure 3.3, and their corresponding parameter values are listed in table 3.5. These results reveal differences in eutrophication sensitivities between the parameterization methods. Fluxes generated by method A were insensitive to eutrophication; in spite of the 32-fold difference in nutrient loading between the 01X and 32X mesocosms, the corresponding fluxes of method A were

virtually identical, fluxing 1711.7 and 1699.6 $\frac{\mu\text{molC}}{\text{cm}^2\text{yr}}$ respectively (see figure 3.3). At most, the POM fluxes differ by a factor of 2.5 in the C05 and 16X mesocosms, with 1032.9 and 2577.0 $\frac{\mu\text{molC}}{\text{cm}^2\text{yr}}$, respectively.

In contrast, joint POM flux parameterizations of methods B, C and D were far more sensitive to eutrophication. Joint method B generated fluxes of 137.4 and 2250.5 $\frac{\mu\text{molC}}{\text{cm}^2\text{yr}}$ in the C01 control and 32X mesocosms, respectively, and joint methods C and D exhibited a similar fifteen-fold increase. The nutrient load sensitivity exhibited by these three parameterizations is inherited from their chlorophyll and zooplankton inputs. Figure 2.4 reveals a strong increase in chlorophyll and zooplankton concentrations as the mesocosms become more eutrophic, a trend which joint methods B, C and D follow in direct proportion.

When methods B, C and D were optimized individually, the POM fluxes closely matched the eutrophication-insensitive fluxes of method A. Examination of the individually optimized parameter values of method B reveals a decreasing trend of parameter values with higher nutrient loads, varying p_{chla} from 209.9 $\frac{\mu\text{molC}}{\text{cm}^2\text{yr}} \frac{L}{\mu\text{gChl}_\text{a}}$ in the C01 mesocosm to 24.5 $\frac{\mu\text{molC}}{\text{cm}^2\text{yr}} \frac{L}{\mu\text{gChl}_\text{a}}$ in 32X. The net effect of this trend reduces the resulting POM flux's sensitivity to eutrophication, producing mean POM fluxes with magnitudes similar to those of method A.

Optimization did not always generate meaningful parameter values. Individual optimizations of methods C and D sometimes resulted in negative parameters which, given the presence of water column phytoplankton or zooplankton, implies a *removal* of organic matter from the sediments. Either this is not a meaningful result, as it completely contradicts the original rationale of the parameterizations, or it's indicative of an unknown removal mechanism which has somehow been implicitly described in the parametrizaiton. Without access to directly measured parameters however, it is not possible to decide between these two possibilities. Although individually optimized methods C and D produced smaller cost functions than when they were jointly optimized, this was only the expected result of the optimizer exploiting the extra degrees of freedom made available by assigning individual parameters to each mesocosm.

The final set of POM flux experiments optimized POM parameterizations for both the two-layer model and multi-layer model by varying sediment model parameters in addition to POM flux parameters. These experiments only examined methods A and B.

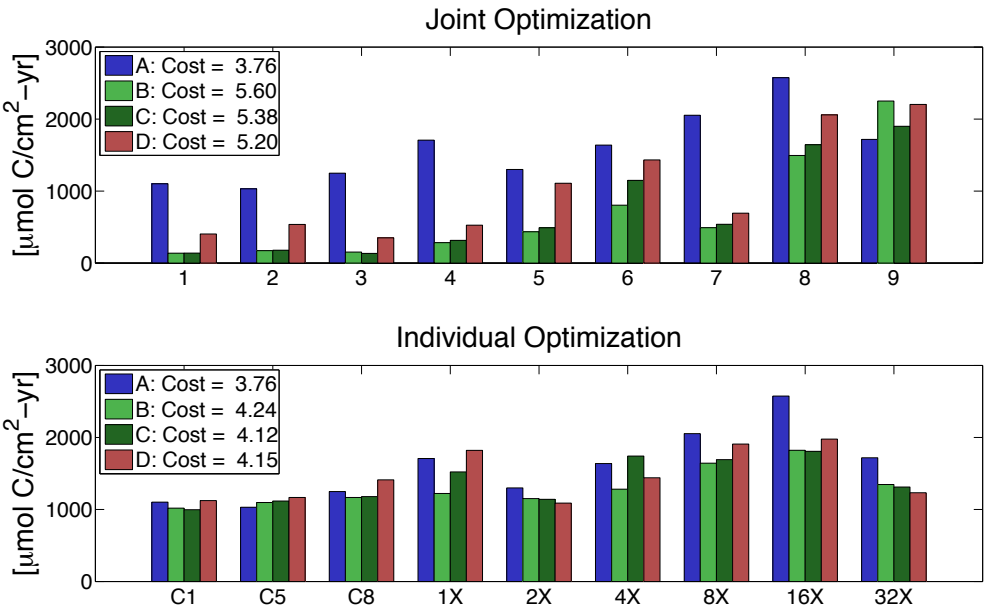

Figure 3.3: POM flux, joint vs. individual parameterizations: Jointly optimized flux parameterizations B, C, and D are sensitive to nutrient loading, while the individually parameterizations are not.

Because so many parameters were being varied, it was necessary to switch from using the gradient descent optimization algorithm, to evolutionary algorithms. Consequently, the cost functions resulting from these optimizations cannot be directly compared to those of the previous POM flux optimizations. The multi-layer model produced costs of $F_{m,A}$ = 3.1$\pm$2.8, and $F_{m,B}$ = 4.2$\pm$2.8, while the two-layer model generated costs of $F_{2,A}$ = 3.1$\pm$2.8 and $F_{2,B}$ = 3.7$\pm$2.8. Uncertainties in the cost are too large to make any comparison, but, ignoring eutrophic mesocosm cost contributions produces costs of $F_{m,A}$ = 0.52$\pm$0.04, and $F_{m,B}$ = 1.3$\pm$0.04 for the multi-layer model, while the two-layer model generated costs of $F_{2,A}$ = 0.85$\pm$0.03 and $F_{2,B}$ = 0.83$\pm$0.04. The multi-layer model thus generates a better fit when accepting a constant POM flux as input as opposed to scaling the flux with chlorophyll. The two-layer model, by including the model parameters in the optimization, appears to be able to perform equally well with the chlorophyll-derived input.

Overall, method A and joint method C produced the smallest cost functions, but these costs were also within the bounds of uncertainty of one another. It was necessary to choose a POM parameterization method for further studies, so methods A was used as its cost was

smaller, and it required no inputs.

3.3 Optimized Model Results

For both the two- and multi-layer models, baseline parameter values were taken from their original publications (*Soetaert et al.*, 1996b; *DiToro*, 2001). Hessian analysis was used to develop a list of parameters to optimize, and these parameters were optimized along with the POM flux parameters. Sediment fluxes calculated by both models were compared to the MERL observations, including the oxygen flux, ammonium flux, nitrate flux, and phosphate flux. Modelled reaction rates of carbon decomposition, nitrification, and denitrification were compared against rate estimates based on an equilibrium model which inferred the reaction rates from observed fluxes. In these time series plots, the model outputs are compared by calculating sum of the squared error (SSE) between output and observation. Otherwise, the models are compared on the basis of a cost function (see methods). A breakdown of the cost contributions according to mesocosm and flux type is given in figure 3.4. Overall costs of the two models, F_2 = 3.09$\pm$2.8 for the two-layer model, and F_m 3.11$\pm$2.8 for the multi-layer model, were within error of one another. The cost function breakdown clearly indicates that over half of the cost comes from the eutrophic mesocosms. As will be discussed later, much of this misfit is derived from noise in the observations, and for this reason, the model costs were re-calculated, this time using the same model outputs, but ignoring contributions from the eutrophic mesocosms. These new costs were F_2 = .85$\pm$.03 and F_m = .53$\pm$.04, and were distinct from one another, with the multi-layer model having a smaller (better) cost and no overlap between each model's bound of uncertainty. These results are still not an entirely fair comparison however, as the parameters of these models have been fit using the noisy observations of eutrophic mesocosm data. If the models are optimized while ignoring the eutrophic mesocosm data entirely, the multi-layer model's cost is still better, i.e., F_m = .47$\pm$.03 versus F_2 = .64$\pm$.03. Interestingly, both models improved, but the two-layer model improved more. This suggests that the two-layer model is less able to handle noise in its inputs. Parameter values resulting from the optimization of both models in all the mesocosms are listed in the appendix (see A.1 and A.2).

The models were evaluated on the basis of four benthic flux outputs, specifically the oxygen, nitrate, ammonium, and phosphorus fluxes. Successful modelling of these fluxes

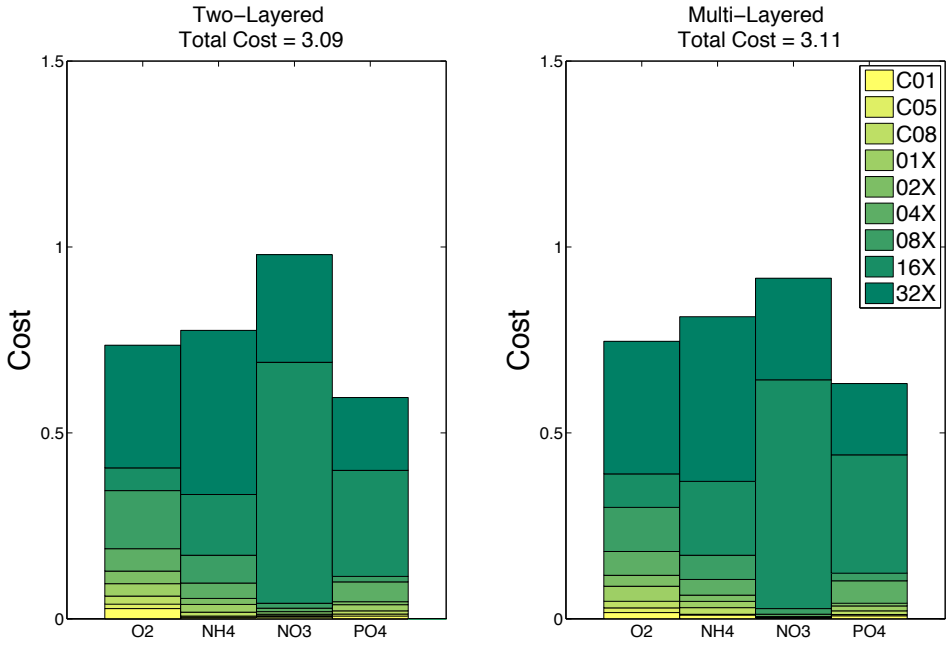

Figure 3.4: Cost function breakdowns of two- and multi-layer models. X-axis identifies flux type, and bar colour identifies mesocosm.

first required the models to accurately estimate carbon metabolism within the sediments. While direct observation of the carbon metabolism was not made in the MERL experiments, it was possible to infer these rates by assuming that the sediment transports and reactions were in steady state (see methods). Rates produced by the equilibrium model exhibited a strong seasonal signal, with larger summer peaks in the more eutrophic mesocosms. Both the two-layer and multi-layer models were able to resolve the timing of this variation by applying an approximated Arrhenius factor to their overall carbon consumption rates (Fig 3.5(a)). The models also varied the consumption rate with carbon availability, and thus, the summer peak rates roughly scaled with the magnitude of the POM flux inputs (Fig 3.6).

The observed and modelled oxygen fluxes in the MERL system (Fig 3.7) were very closely related to the rates of metabolized carbon, exhibiting the same seasonal variation, and summer peaks which roughly scaled with the POM flux inputs. Generally speaking, there exists a close relationship between the consumption rates of oxygen and carbon. When carbon is consumed, this may occur through the aerobic metabolism that consumes oxygen directly, or an anaerobic metabolism which generates reduced products that then

react with oxygen. Both chemical pathways consume the same ratio of carbon to oxygen, and thus their consumption rates are closely related.

Presumably, it is for this reason that the two-layer model does not explicitly describe an aerobic carbon metabolism. Instead, oxygen consumption in the sediments are indirectly handled by the sulphate reduction metabolism. When consuming a quantity of carbon, this metabolism generates H_2S, which rapidly reacts with oxygen. Most anaerobic metabolisms produce reduced intermediates that function in this way, although denitrification is an exception. Denitrification generates N_2 gas, which is highly inert and can only be oxidized under special conditions.

The multi-layer model experienced some problems in recreating the large summer oxygen fluxes. In order to produce a large flux, it was necessary to resolve a sharp oxygen gradient near the sediment surface. This was accomplished by placing many thin layers near the surface and allowing layer thickness to increase with depth. However, since the model was being integrated using a Euler-forward scheme, the maximum timestep size shrank with the square of the smallest layer thickness. The resulting timestep, .0005 days, slowed down the model notably, requiring slightly over two minutes to complete the 2.5 year simulation. In contrast, the two-layer model was able to perform the same simulation in only a few seconds.

The multi-layer model also experienced another related problem: it was unable to oxidize sufficient ODUs (oxygen debt units, the reduced product of the model's anaerobic metabolism) before they diffused from the sediment. This ODU outflux essentially can be thought of as an outflux of H_2S, which is not at all characteristic of a well oxygenated environment. This outflux also affects the sediment oxygen flux: when ODUs escape the sediment, there is less demand for oxygen within the sediment, and the resulting influx of oxygen is smaller. It was found that a more realistic oxygen flux was generated when the ODU flux was subtracted from the unmodified oxygen flux. Creating this modified oxygen flux essentially assumes that all the ODUs were consumed inside the sediments in spite of how the model behaved. Since this modified oxygen flux improved the model's fit, all the multi-layer model's oxygen flux results in this thesis have been adjusted in this manner.

Observed ammonium fluxes (Fig 3.8) exhibited strong seasonal variation in all mesocosms, with peak summer fluxes scaling roughly with the mesocosm's POM input. During winter, fluxes became very small, and in the case of the 8x, 16x and 32x mesocosms, fluxes

even became negative. The uncertainties of the fluxes in these mesocosms are very large, and the timing of the negative fluxes is difficult to discern. After being fit to this data, both the multi-layer model and the two-layer model succeed in producing negative fluxes in these mesocosms, but exhibited a different timing. Also, the models' magnitude of the influxes tends to be smaller than observed, although well within uncertainty for the eutrophic mesocosms. In general, both models were able to capture the regular seasonal behaviour evident in most mesocosms; however, observed variation within the 32x mesocosm broke from the seasonal pattern, and the models were unable to capture this signal. As a result, the ammonium flux's cost contribution is dominated by the 16x and 32x mesocosms (see Fig 3.4).

Observations of the nitrate flux did not exhibit any distinctive signal and generally fluctuated around zero. In the less eutrophic mesocosms, the models reproduced this behaviour quite well (Fig 3.9). In the more eutrophic mesocosms, the observed nitrate fluxes appear to become more noisy, and there was no discernible signal for the models to reproduce. The eutrophic mesocosm fluxes had high uncertainties, and the models were being optimized to fit these noisy observations. This of course did result in a good fit, and neither model succeeded in reducing the nitrate flux's cost contribution significantly below the baseline value of 1. Indeed, the plotted cost breakdown (Fig 3.4), shows that the majority of the nitrate cost contributions come from the eutrophic mesocosms.

Nitrification estimates of both layered models were not as large as those of the equilibrium model, and neither did they follow the reaction's time-variation (Fig 3.10). This was particularly true for the 32x mesocosm and is likely a symptom of the noisy flux observations. A similar mismatch also existed within both layered models' and equilibrium model's denitrification rates (Fig 3.11). Notably, the denitrification rates of the equilibrium model do not seem reliable in the eutrophic mesocosms: the estimates come with large uncertainties. The equilibrium model also produces negative reaction rates within the eutrophic mesocosms.

Phosphate fluxes (Fig 3.12) were generally observed to follow the seasonal signal of the carbon metabolism, and in the less eutrophic mesocosms, layered models capture this behaviour. In the 16x and 32x mesocosms, the two-layer model captures some irregularities in the flux by sorbing solid phophate into the sediment when oxygen concentrations are high and releasing phosphate when oxygen concentrations drop. The multi-layer model,

although capable of sorbing phosphate in this way, did not exhibit this behaviour because Hessian analysis indicated its relevant phosphate parameters to be correlated, and these parameters were removed from the optimization process. In spite of the noise in the observed eutrophic phosphate fluxes, the phosphate cost contributions are the smallest of all the model outputs. However, over three quarters of the cost contribution come from 16x and 32x.

The carbon metabolism was the only model output where the unmodified sum of the squared error (SSE) was sufficiently different between the two models to be distinguishable (i.e. they were not within error of each other). When eutrophic mesocosm cost contributions were not included in the cost calculation, or if their data was used during optimization, the multi-layer model frequently performed better than the two-layer model (see tables 3.6 and 3.7). Table 3.8, summarizes this comparison between models.

3.4 Oxygen Flux Parameterizations

Two oxygen flux parameterizations were fit to the MERL data using a non-linear regression algorithm (Fig 3.13), and these were compared to the oxygen flux outputs of the two- and multi-layer models (Fig 3.14). The two parameterizations used were from *Murrell and Lehrter* (2010) (referred to as ML10), which produced an oxygen flux that varied linearly with overlying water column oxygen, and from *Hetland and DiMarco* (2008) (referred to as HD08), which included an Arrhenius factor and an oxygen limitation factor.

These simple parameterizations are not as versatile as the more complex layered models and produced a larger misfit of 2.59$\pm$.07 for the ML10, and 0.78$\pm$.04 for the HD08 parameterization. The layered models on the other hand, produced smaller, better costs of 0.67$\pm$.04 for the two-layer model, and 0.61$\pm$0.04 for the multi-layer model. The ML10 parameterization was particularly ill-suited to the MERL system, producing seasonal oxygen fluxes which were entirely out of phase with observations. The HD08 parameterization had a significantly better fit, using its temperature sensitivity to capture the oxygen flux's seasonal variation. Since the mesocosm water columns were always well oxygenated, the HD08 parameterization's oxygen-dependent parameter remained un-constrained.

3.5 Cross Validation

Ideally, a process oriented sediment model should be capable of functioning in multiple environments without modifying its parameter set. Were this to be the case, fitting the sediment models to one set of observations would simultaneously improve the models' fit with a second independent set of observations, or at least not have a negative effect on the fit. In cross validation experiments, the sediment model parameters were fit to a subset of observations from the MERL mesocosms. Then, the resulting parameter set was tested within all of the MERL mesocosms.

Ten of such optimizations were performed, and the resulting cost functions were averaged. The multi-layer model generated an average cost of 3.37 $\pm$ 2.8, while the two-layer model averaged at 4.08 $\pm$ 2.8. The average cost function is smaller in the multi-layer model, indicating it may be less prone to overfitting, but the difference between both models is inconclusive since it is smaller than the uncertainty. When the eutrophic mesocosms are ignored, the average costs drop to 0.57$\pm$0.03 for the two-layer model and 0.40$\pm$0.03 for the multi-layer model. The multi-layer model, having the better score, therefore seems to be less affected by being fit to the noise in the eutrophic mesocosms.

Another identical cross validation experiment was performed on the Hetland & DiMarco parameterization, which had an averaged oxygen flux cost contributions of 0.83 $\pm.04$. In comparison, the cross validation experiments for the layer models generated oxygen flux cost contributions of 0.70 $\pm.04$ for the multi-layer model and 1.11 $\pm.04$ for the two-layer model. Note that this particular experiment did not require ignoring the cost contributions from the eutrophic mesocosms as the oxygen data contains relatively little noise.

Table 3.5: Two-layer model parameter values for depositional flux parameterizations.

	Method A	**Method B**
Optimization	p_{const}, $\left[\frac{\mu\text{molC}}{\text{cm}^2\text{yr}}\right]$	p_{chla}, $\left[\frac{\mu\text{molC}}{\text{cm}^2\text{yr}}\frac{L}{\mu\text{gChl}_\text{a}}\right]$
Joint	-	37.1
C01	1119.2	209.9
C05	1032.9	179.8
C08	1271.2	219.5
01X	1711.7	157.2
02X	1292.0	78.1
04X	1639.1	62.7
08X	2064.0	104.8
16X	2577.0	54.8
32X	1699.6	24.5

	Method C	
Optimization	p_{dia}, $\left[\frac{\mu\text{molC}}{\text{cm}^2\text{yr}}\frac{L}{\mu\text{gChl}_\text{a}}\right]$	p_{other}, $\left[\frac{\mu\text{molC}}{\text{cm}^2\text{yr}}\frac{L}{\mu\text{gChl}_\text{a}}\right]$
Joint	23.5	78.6
C01	188.6	50.5
C05	261.7	146.5
C08	209.2	678.5
01X	320.2	-107.6
02X	90.5	102.1
04X	169.1	-11.5
08X	150.4	57.9
16X	42.3	4.6
32X	23.8	-33.7

	Method D	
Optimization	p_{chla}, $\left[\frac{\mu\text{molC}}{\text{cm}^2\text{yr}}\frac{L}{\mu\text{gChl}_\text{a}}\right]$	p_{zoo}, $\left[\frac{\mu\text{molC}}{\text{cm}^2\text{yr}}\frac{L}{\text{dry}\mu\text{gzoopl.}}\right]$
Joint	27.2	5.3
C01	44.7	17.0
C05	46.1	12.4
C08	46.8	27.8
01X	45.0	25.4
02X	60.3	12.5
04X	54.4	1.5
08X	107.1	7.4
16X	38.5	2.2
32X	23.0	-2.4

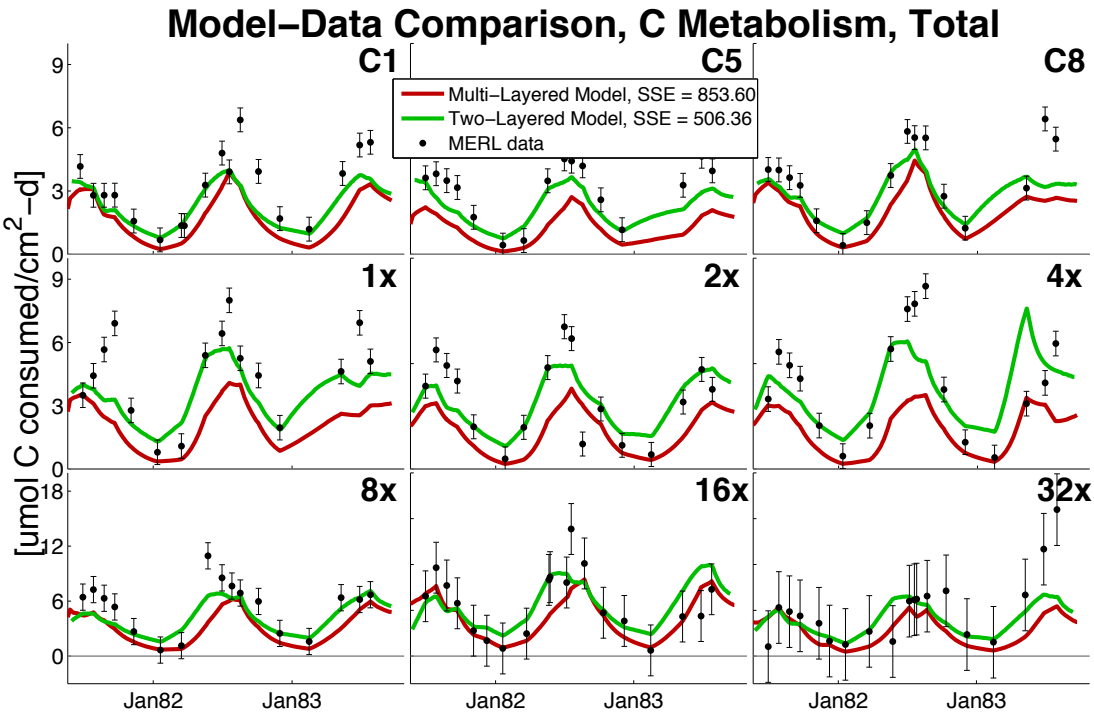

(a) Carbon metabolism, modelled and inferred from observation. Metabolic rates are highly seasonal, and controlled by temperature. Note the change in y-axis scale for the eutrophic mesocosms.

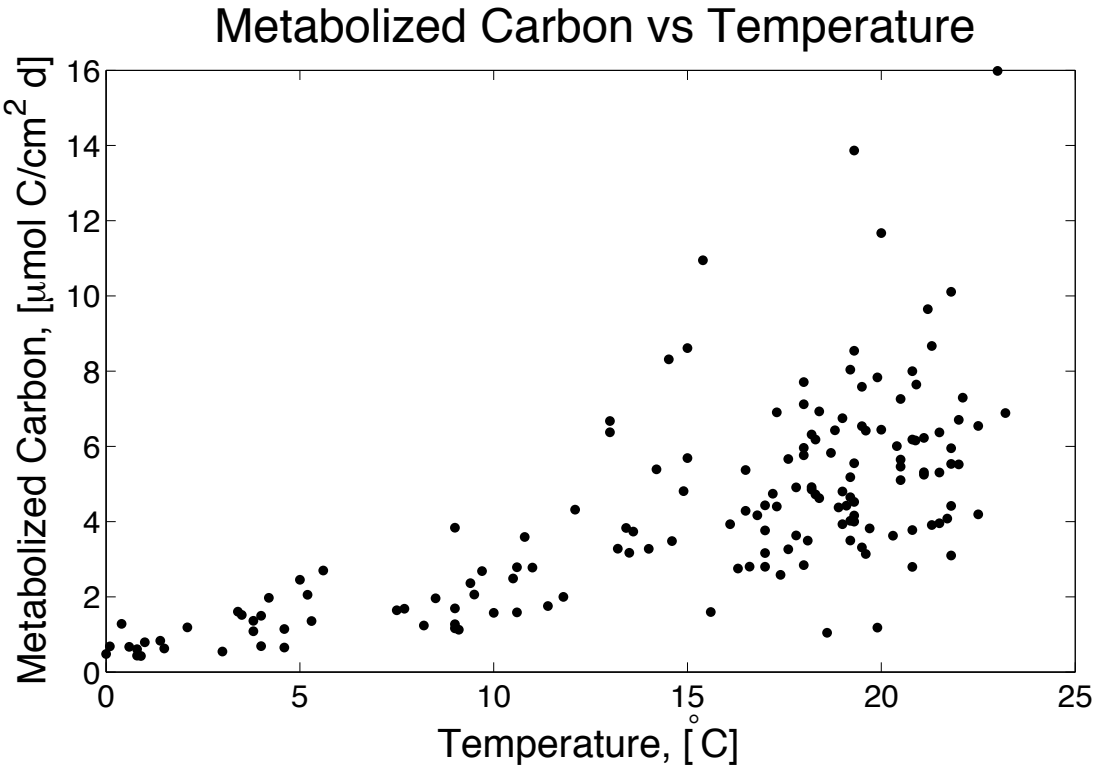

(b) Carbon metabolism vs temperature

Figure 3.5: Total Carbon Metabolism. The metabolic rate is dependent on temperature. R^2 = 0.469

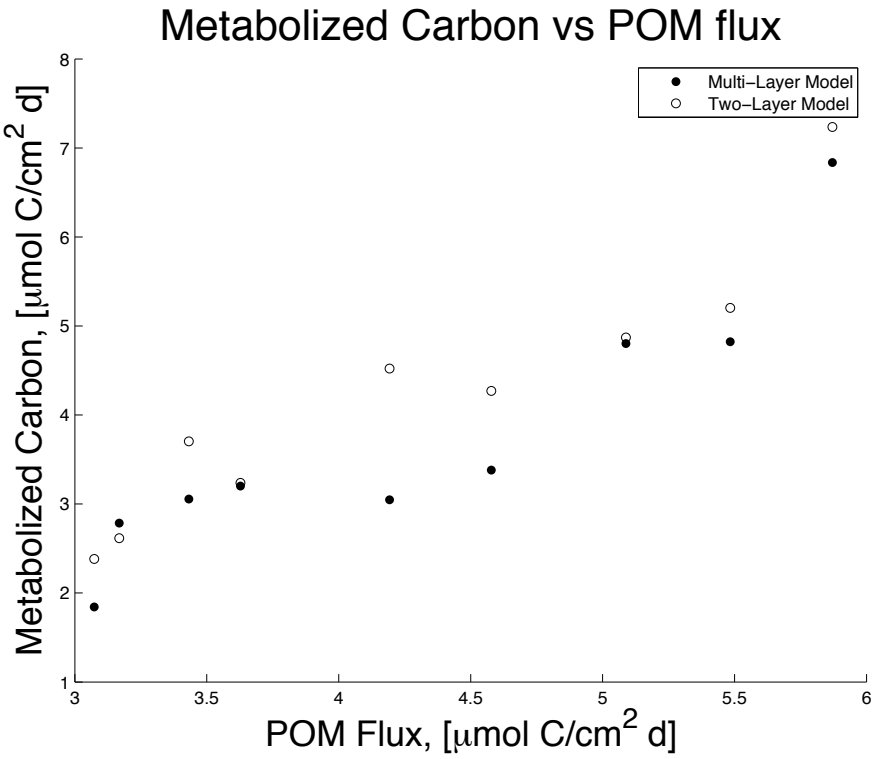

Figure 3.6: Carbon metabolism vs depositional flux of particulate organic matter: the two are strongly correlated for both layered models. Multi-layer model $R^2 = 0.842$, two-layer model $R^2 = 0.881$

Table 3.6: Two-layer model: sum squared error, each output

Output	Eutrophic mesocosms contribute to cost function	Eutrophic mesocosms ignored in cost function	Eutrophic mesocosms ignored during optimization
O_2 flux	663 $\pm$33	410 $\pm$26	306 $\pm$23
NH_4 flux	25 $\pm$14	7.5 $\pm$0.8	5.6 $\pm$0.7
NO_3 flux	29 $\pm$83	0.94 $\pm$0.17	0.61 $\pm$0.15
PO_4 flux	0.47 $\pm$0.14	0.11 $\pm$0.006	0.09 $\pm$0.005
C metabolism	506 $\pm$156	407 $\pm$22	319 $\pm$20
Denitrification	119 $\pm$203	6.9 $\pm$1.2	6.2 $\pm$1.1
Nitrification	139 $\pm$65	13.9 $\pm$2.5	13.3 $\pm$2.5

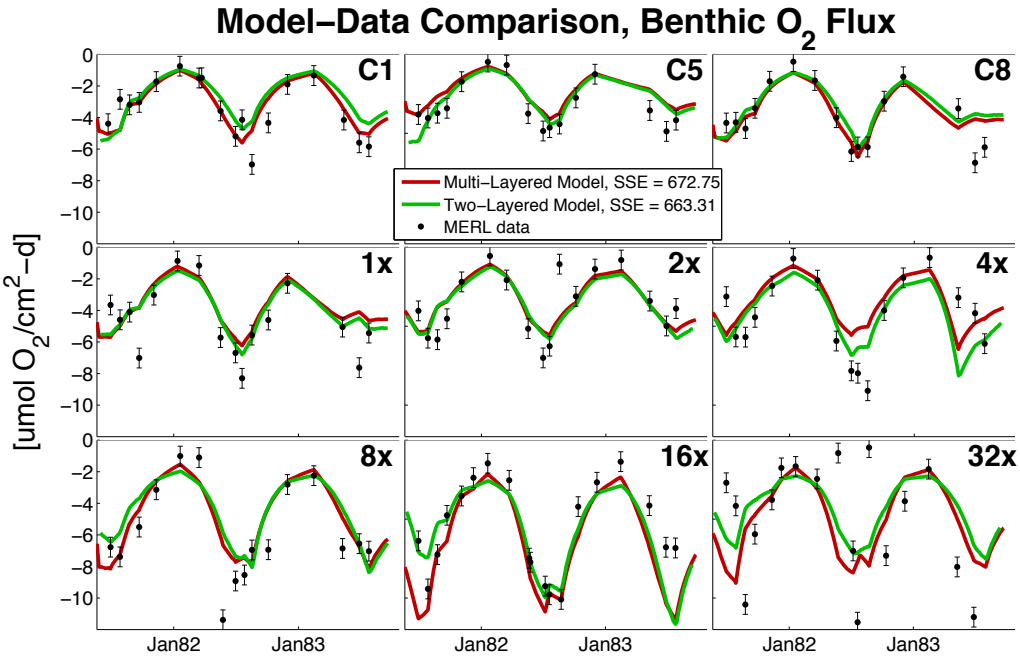

Figure 3.7: Oxygen fluxes, modelled and observed. The fluxes almost double in magnitude up the eutrophication gradient.

Table 3.7: Multi-layer model: sum squared error, each output

Output	Eutrophic mesocosms contribute to cost function	Eutrophic mesocosms ignored in cost function	Eutrophic mesocosms ignored during optimization
O_2 flux	672±34	239±20	229±20
NH_4 flux	27±15	4.4±0.63	3.7±0.62
NO_3 flux	27±83	0.39±0.14	0.34±0.13
PO_4 flux	0.51±0.15	0.093±0.005	0.07±0.005
C metabolism	853±174	470±25	484±25
Denitrification	111±203	6.1±1.2	5.3±1.1
Nitrification	146±67	15.3±2.6	13.7±2.5

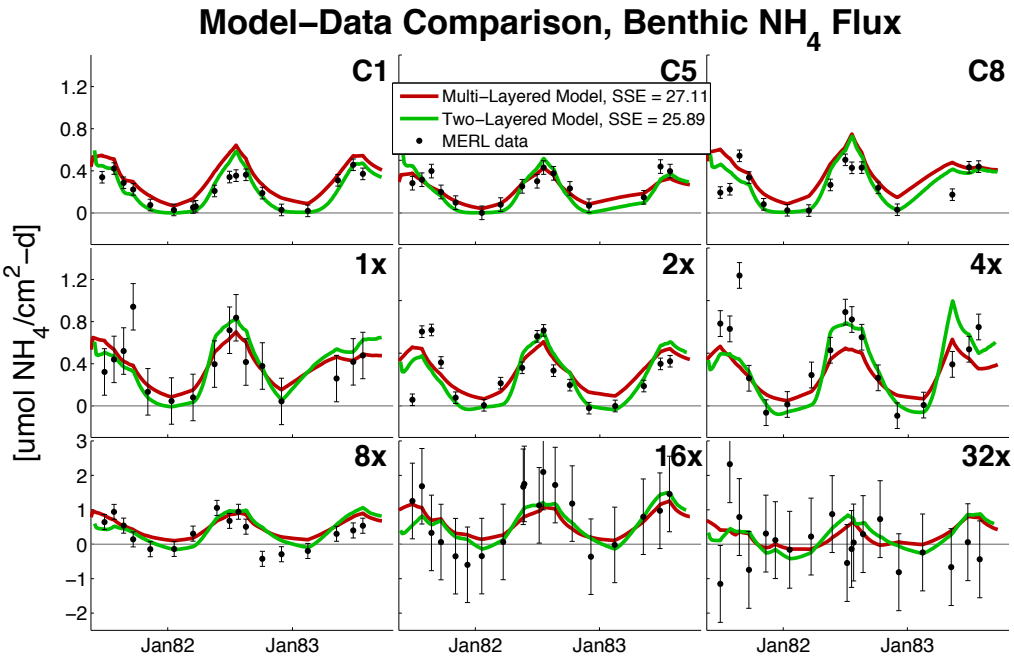

Figure 3.8: Ammonium fluxes, modelled and observed. Noise in the eutrophic mesocosms conceals any discernible signal. Note the change in y-axis scale for the eutrophic mesocosms.

Table 3.8: Comparison of the two- and multi-layer model SSE. When both models generate an SSE within the bounds of uncerertainty of the other, it is noted as ”tie”. Otherwise, the model with the superior SSE is noted.

Output	Eutrophic mesocosms contribute to cost function	Eutrophic mesocosms ignored in cost function	Eutrophic mesocosms ignored during optimization
O_2 flux	Tie	Multi-Layer	Multi-Layer
NH_4 flux	Tie	Multi-Layer	Multi-Layer
NO_3 flux	Tie	Tie	Multi-Layer
PO_4 flux	Tie	Multi-Layer	Multi-Layer
C metabolism	Two-Layer	Two-Layer	Two-Layer
Denitrification	Tie	Tie	Tie
Nitrification	Tie	Tie	Tie

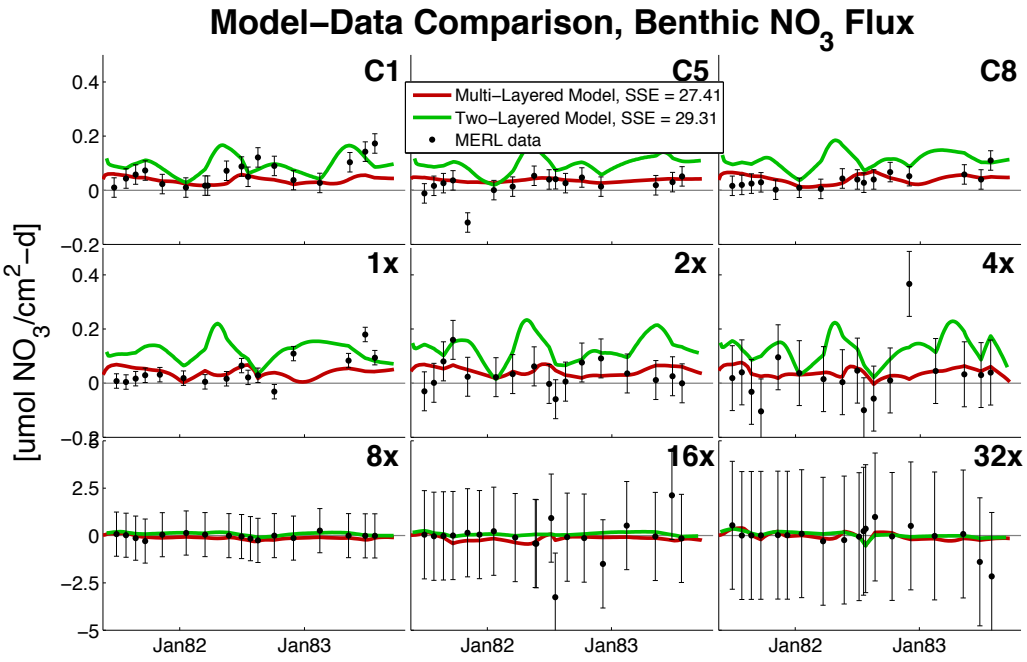

Figure 3.9: Nitrate flux, modelled and observed. Both models produce very small denitrification rates. The observed fluxes wildly fluctuate in the eutrophic mesocosms, but have large uncertainty, and so could easily be close to zero like the other mesocosms.

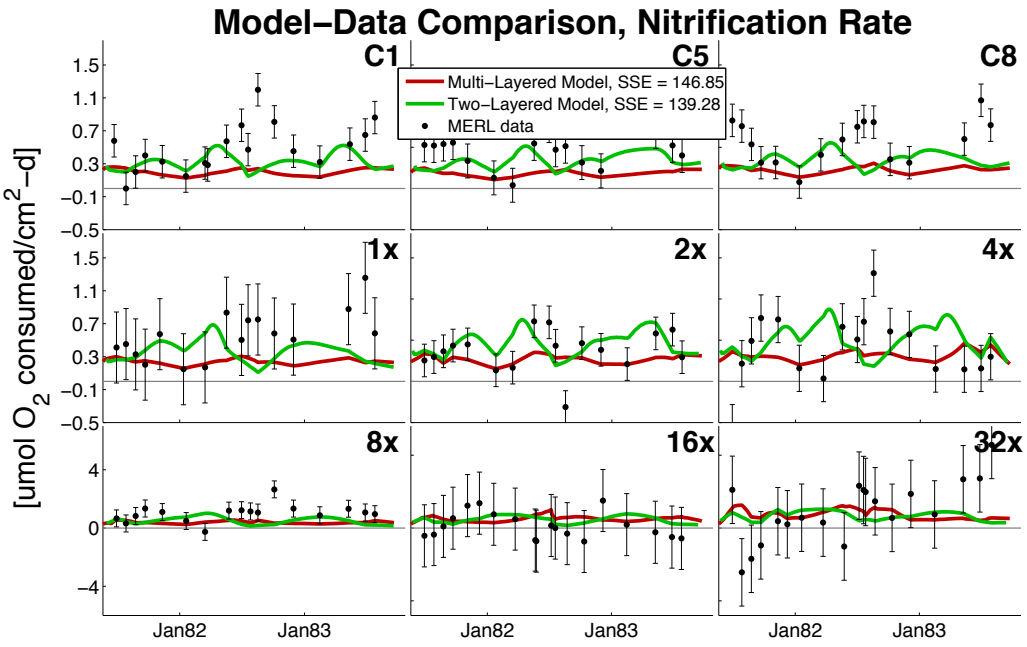

Figure 3.10: Nitrification rates, modelled and inferred from observation. Note the change in y-axis scale for the eutrophic mesocosms.

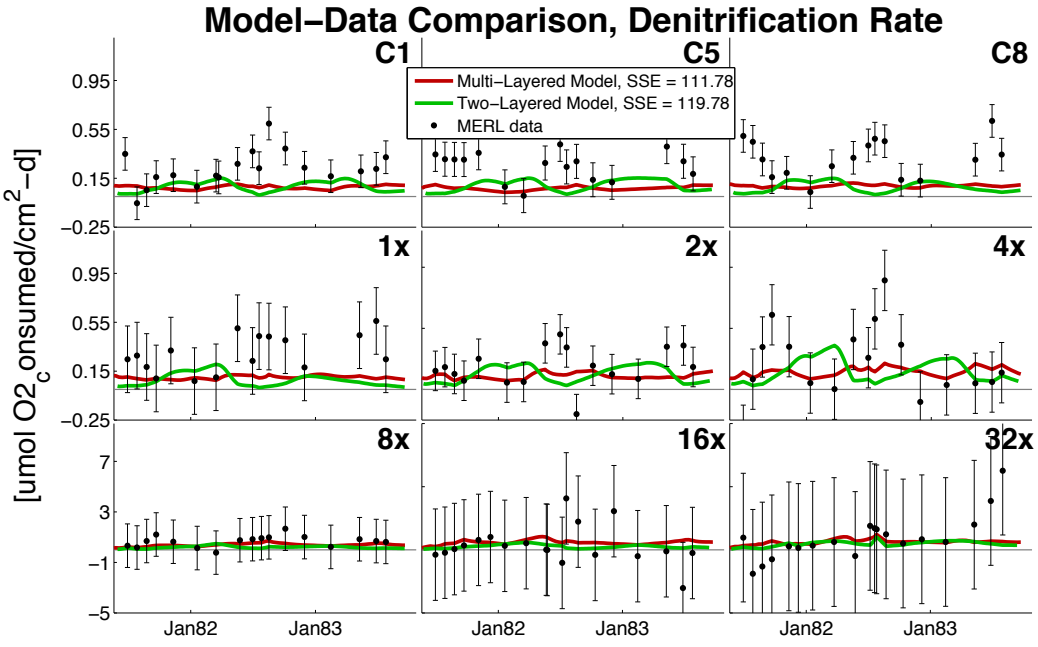

Figure 3.11: Denitrification rates, modelled and inferred from observation. Models consistendly underestimate denitrification rates in the less eutrophic mesocosms. Uncertainty in the eutrophic rates are very large, rendering these rates indistinguishable from the models. Note the change in y-axis scale for the eutrophic mesocosms.

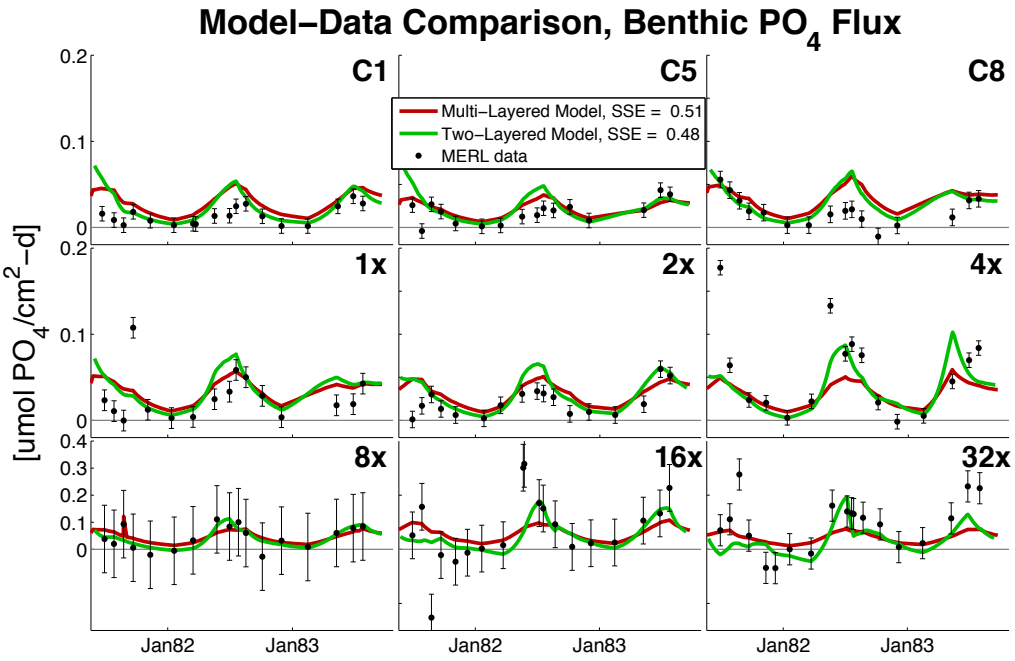

Figure 3.12: Phosphate flux, modelled and observed. Observed fluxes suggest influxes of phosphate into the sediment. Uncertainty in these observations are large, but models somewhat recreate this behaviour

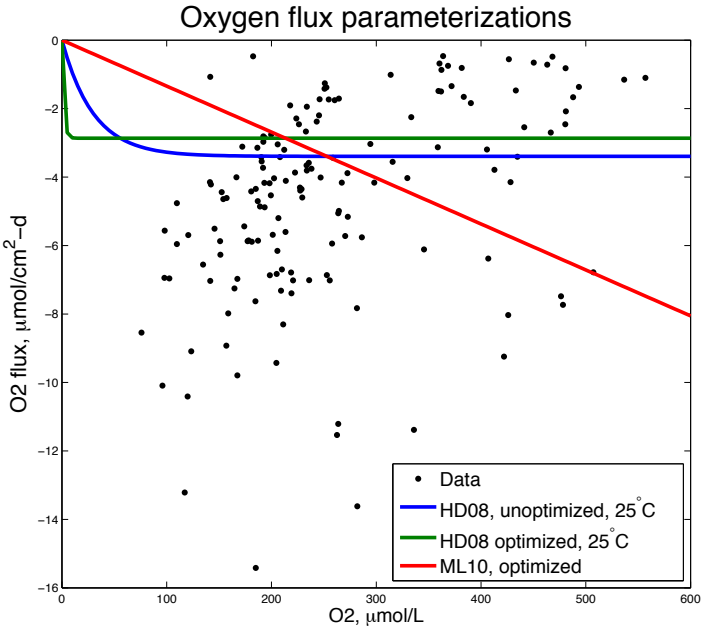

Figure 3.13: Sediment oxygen demand and oxygen concentration scatter plot: parameterizations and MERL data

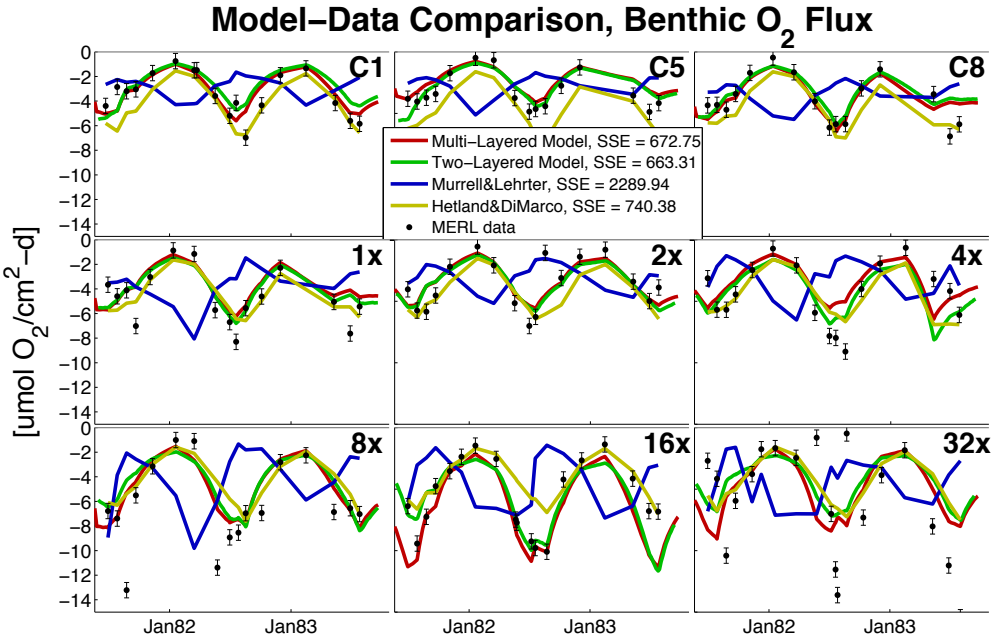

Figure 3.14: Oxygen fluxes generated by models and parameterizations.

CHAPTER 4

DISCUSSION

4.1 POM Flux Parameterizations

Among the first steps of this study was to determine an unknown model input, the depositional flux of particulate organic matter (POM flux). This flux is ultimately derived from biomass within the water column, so it is reasonable to expect that the former scales with the latter. Following this line of reasoning, POM flux parameterization methods B, C and D generate a POM flux in proportion to proxies of water column biomass, specifically, chlorophyll a, diatom abundance, and/or zooplankton concentrations. Likewise, virtually all conventional water column models use similar linear or quadratic relationships. By positing a linear relationship between POM flux and water column biomass, two outcomes can be expected: first, because water column biomass grows with the availability of inorganic nutrients, it follows that the largest POM fluxes are expected to take place in the more eutrophic MERL mesocosms; second, seasonal variation in the water column would result in seasonal variation of the POM flux.

Parameterizations B, C and D, when optimizing a universal parameter set to fit all of the mesocosms (i.e. when jointly implemented), produced POM fluxes which roughly scaled with eutrophication, as expected. An improved fit was achieved when these same methods assigned a different parameter set for each mesocosm (i.e. when individually implemented). In this case, the mean POM fluxes did not follow the expected trend along the eutrophication gradient, but instead varied relatively little across all mesocosms. Method A, which assigns a constant individual POM flux to each mesocosm, generated a similar eutrophication-insensitive result. The resulting fits of method A were within

uncertainty or better than those of the individual parameterizations B, C and D. Thus, contrary to expectation, the parameterizations that resulted in the best fit were also the least sensitive to nutrient-loading.

This result is also contrary to our second expectation, that is, when the POM fluxes were constant, the model's fit was as good or better than if the POM flux varied with seasonal biomass signals. This suggests that variation of the true POM flux signal may have been out of phase with that of the water column biomass, or it may have been of a smaller amplitude, or a combination of the two.

Neither of these divergences from expectation appear to be the result of poorly tuned sediment model parameters, for when these parameters were included in the optimization process, the same result was achieved. It is also unlikely that the results are due to a systematic bias in either of the models, because both the two-layer model and the multi-layer model generated a similar result, although the possibility that both models share the same bias hasn't been eliminated.

It is worth noting that sediment resuspension occurred throughout the experiment. Movement of the the stirring plungers within the mesocosms was calibrated to resuspend sediment until it reached concentrations similar to that of Narragansett Bay (i.e. 3 $\frac{\mathrm{mg}}{\mathrm{L}}$); however, the organic fraction of this resuspended sediment would be directly related to the concentration of organic matter at the sediment surface, which in turn is related to the POM deposition rate. Should eutrophication indeed induce an increased rate of POM deposition, a greater amount of organic matter would also be resuspended, and therefore subjected to removal by decomposition within the water column. Thus, sediment resuspension would serve to reduce the POM flux's observed sensitivity to eutrophication, possibly resulting in the eutrophication-insensitive POM fluxes generated by method A, and the independently optimized methods B, C, and D.

A break-down of the model's cost contributions clearly shows that the eutrophic mesocosms consistently dominate the cost function. When optimizing a joint POM parameterization, the less eutrophic mesocosms would, therefore, be using parameters that are better suited to the more eutrophic ones. As discussed above, the effects of resuspension likely induced a negative POM flux bias, which roughly scales with mesocosm eutrophication. When methods B, C and D are optimized jointly, the large negative bias of the eutrophic mesocosms would be imposed on the less eutrophic mesocosms, and their

POM flux estimation would be far too small. Indeed, our results revealed a significant increase of POM flux within the less eutrophic mesocosms once methods B, C and D were optimized individually.

Sediment resuspension would also reduce seasonal variation within the POM flux. As discussed above, this effect reduces the POM flux's sensitivity to water-column biomass concentrations. The observed POM flux would depend less on the seasonal biomass signal, and more on the rate of resuspension. Since the mesocosm mixing plungers churned the water at constant intervals, the rate of sediment resuspension also would have been relatively constant. Thus, these effects could account for method A achieving the overall lowest cost.

It is unfortunate that sediment resuspension appears to produce such a profound bias in the POM flux parameterizations, as it also renders the use of sediment traps problematic. Without reliable empirical observations or a parameterization that is well-grounded in theory, resuspension will hinder the quantification of this important model input. This problem can be side-stepped in future studies by choosing to simulate regions where resuspension is not a significant factor. If this is not possible, a sediment model may better resolve the POM flux by modelling the resuspension and transport of sediment.

4.2 Optimized Model Results

The multi-layer model and two-layer model are both constructed around a different design philosophy—one is vertically integrated, and the other is vertically resolved—so it was not expected that the fitted model outputs would resemble one another so closely (Fig 3.4). The costs are similar in almost every respect, whether cost contributions are broken down according to the model output, or mesocosm. Unless the cost contributions of mesocosms 8X, 16X and 32X are excluded from the final cost calculation, the model costs are within error of each other. When observations from those eutrophic mesocosms are excluded entirely from optimization, the models' still differ beyond the margin of uncertainty, but the margin is smaller.

There are reasons to expect that the models might behave similarly. Both models simulate the same chemical processes (albeit sometimes under different labels). Both simulate denitrification and nitrification. The two-layer model simulates the anaerobic sulphate metabolism, and the oxidation of H_2S, and the multi-layer model simulates an

analagous anaerobic metabolism which generates ODUs which may be oxidized in aerobic layers. While only the multi-layer model explicitly describes an aerobic metabolism, this distinction has very little effect on the model's overall behaviour. The two-layer model and the multi-layer both add any outfluxes of H_2S/ODUs to their oxygen influx estimates. Since this conversion consumes the same amount of oxygen per mole of decomposed carbon, it effectively erases any distinction between an aerobic or anaerobic metabolism, and instead it directly links the oxygen flux to the rate of carbon decomposition.

Similarities between the two model cost contributions may also result from the stability of the oxygen concentrations in the mesocosms. Had low oxygen conditions occurred, they would have induced different non-linear responses in the two models. For example, in order for the two-layer model to represent the effects of oxygen on denitrification rates, it provides a different denitrification parameter to the upper and lower layers: reaction velocity kapp1no3s for the upper layer, and rate constant k2no3s. Changes in oxygen concentrations would change the thickness of the aerobic layer, and thus modify the ratio of aerobic and anaerobic denitrification. Also, changes in oxygen would affect nitrification rates, which would modify the availability of NO_3 for denitrification. The multi-layer model, rather than using two parameter values for denitrification, tries to resolve denitrificaiton rates through representation of the oxygen and denitrification distributions within the sediment. It first estimates a total rate of carbon decomposition, and then attributes $limNO_3 = \frac{\frac{[\mathrm{NO_3}]}{[\mathrm{NO_3}]+k_{s(\mathrm{NO_3})}} \frac{k_{in(O_2denit)}}{[O_2]+k_{in(O_2denit)}}}{\mathrm{lim}}$ of the consumed carbon to denitrification in each layer (see methods section). Because denitrification is less thermodynamically favourable than aerobic decomposition, the multi-layer model includes an oxygen inhibition factor $\frac{k_{in(O_2denit)}}{[O_2]+k_{in(O_2denit)}}$ in this denitrification partitioning. This factor greatly reduces denitrification rates in the aerobic layer, and denitrification mostly takes place just below the oxygenated suface layers, where O_2 is low and NO_3 is high. When water column oxygen levels drop, the depth to which oxygen diffuses into the sediment decreases, which in turn would lower nitrification rates and decrease nitrate supply for denitrification. However, the model's oxygen inhibition factor would also be smaller, increasing the denitrification rate. Since oxygen levels were stable throughout the experiment, neither model was able to differentiate themselves with their unique non-linear denitrification response.

The models did differ in their ability to capture rates of carbon decomposition. The two-layer model produced a significantly smaller sum of squared error (SSE) for this

reaction rate than the multi-layer model, when eutrophic mesocosms were excluded from the calculation. This was the only model output where both models were not within observational error of one another. This result was in spite of the similarities in the two models' temperature-sensitive calculation of the carbon metabolism. Figure 3.5(b) clearly indicates that the MERL carbon metabolism is temperature sensitive, and both models recreate this behaviour by including the same Arrhenius factor in their rate calculations. Differences in the the two models' representation of carbon lability classes was superficial: while the two-layer model uses three lability classes of carbon (the multi-layer model uses two), the inert G_3 decomposes so slowly, it cannot be relevant on the timescale of the MERL experiments. While the two models do differ in their representation of solid transport within the sediments, this likely is not what distinguishes the two-layer model from the other, as the two-layer model is not as finely resolved, and therefore would be at a disadvantage. The two sediment models do differ in the dynamics of their chemistry, so it is possible that the two-layer model is simply better equipped to reconstruct carbon decomposition rates from observed fluxes. When the layer models were optimized while omitting the eutrophic mesocosm data, the two-layer model still produced the best carbon metabolism rates. Therefore, it does not appear that the noise in the eutrophic mesocosms' nutrient fluxes happened to favour the two-layer model output.

Unlike the two models' carbon metabolism, uncertainties in the models' denitrification SSE were too large to allow for comparison. Although the models' output and the MERL estimates were usually within error of one another, the model outputs appeared to be subjected to a negative bias (Fig 3.11). Since the eutrophic mesocosms dominate the cost functions with noisy data, it is possible that optimization generated a parameter set which is inappropriate for the less eutrophic mesocosms, at least so far as denitrification is concerned. It is worth noting that the optimization of the multi-layer model did not involve any parameter that was specifically purposed for calculation of denitrification, but anything remotely related to denitrification was removed either as an insensitive or correlated parameter. Instead, parameters such as diffusion constants and carbon remineralization rates were optimized, but these would only have had indirect effects on the denitrification rates.

It is possible that the multi-layer model's production of ODU outfluxes is affecting the model's ability to compute a proper denitrification rate. By converting the ODU outfluxes

to an O_2 influx, any reduced end-product of the anaerobic metabolism is oxidized and represented in the model output. However this does not address a different issue: that the oxidization ought to take place within the sediment. The thickness of the oxygen surface gradient is inversely related to the rate of sediment oxygen consumption. Therefore, prior to converting the ODU outflux to an O_2 influx, the modelled consumption of oxygen in the sediment was too small, and all else being equal, the oxygen penetration into the sediment is therefore too deep. In effect, if the oxidation of ODUs is relocated to occur inside the sediments, the oxygen distribution within the sediments is changed, and as discussed above, this would have an effect on estimates of denitrification.

Denitrification can be classified into two kinds according to the source of the nitrate: "coupled" denitrification utilizes the nitrate produced by nitrification, while "direct" denitrification consumes nitrate which has diffused into the sediments from the overlying water. Should a supply of nitrate increase in the overlying water, one would expect there to be a greater tendency for direct denitrification to take place. Estimates of the ratio of coupled and direct denitrification are given in figure 4.1. Indeed, direct denitrification is only taking place in the three most eutrophic mesocosms, accounting for approximately 20% of their total denitrification. In order for direct denitrification to take place, nitrate needs to diffuse into the sediment. Both models, with varying degrees of success, produce the necessary influxes in the eutrophic mesocosms 3.9.

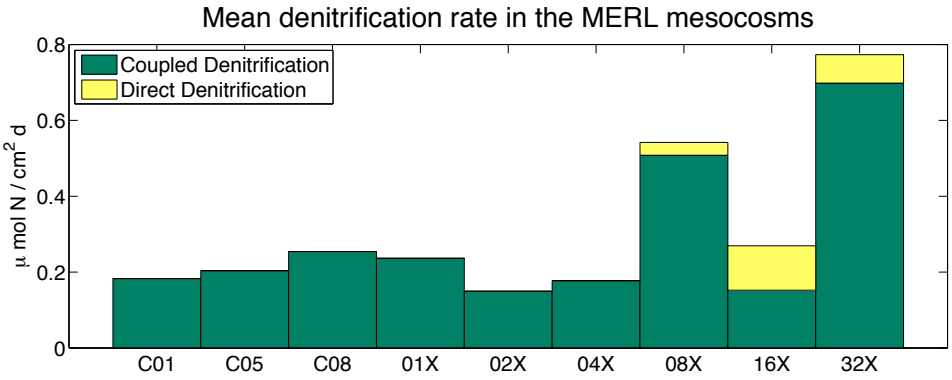

Figure 4.1: Coupled and direct denitrification in the MERL mesocosms.

Another curious trend is the tendency for eutrophic mesocosm sediments to have influxes of ammonium during the winter. While it is unclear whether or not these negative fluxes are merely products of observational noise, the models were able to re-create these

negative fluxes due to a number of contributing factors. First, nitrification was constantly consuming ammonium within the sediment. Second, the ammonium concentrations in a mesocosm's overlying water column scaled in approximate proportion to that mesocosm's nutrient loading. Third, the depositional POM flux in a mesocosm did not scale with the mesocosm's nutrient load, but varied very little by comparison. Thus, the ratio of overlying water column ammonium to remineralized ammonium in the sediment grew dramatically in the more eutrophic mesocosms. When the ratio became sufficiently large, winter concentrations of ammonium in the water column became larger than the sediment concentrations, and ammonium fluxed into the sediment. These negative fluxes were sustained over the winter seasons as ammonium was consumed by sediment nitrification.

The phosphate fluxes of the two models are interesting, in that the multi-layer model produced a SSE which was equal to or better than the two-layer model, depending on how the SSE was calculated. This is despite of the fact that only the two-layer model included phosphate partitioning parameters in its optimization. These parameters are used to describe a phosphate sorbtion mechanism: under oxic conditions, phosphate sorbs to metal oxides and is trapped within the solid phase of the sediments, and when oxygen concentrations drop (or oxygen doesn't penetrate as deeply), some of the sorbed phosphate is released and fluxes back out from the sediment. Although the multi-layer model had the capacity to describe this behaviour, Hessian analysis of the multi-layer model parameters required the removal of all phosphate storage parameters. Referring to figure 3.12, it is evident that the multi-layer model's phosphate flux is varying primarily with carbon metabolism and is not undergoing any complex interactions. In contrast, the two-layer model is seen to draw phosphate into the sediments where it is stored for a time, and then released in a large outflux spike. It is likely that the two-layer model was not able to fully exploit this advantage, because phosphate storage became most significant in the eutrophic mesocosms, which also happens to be where the data becomes the most noisy.

4.3 Oxygen Flux Parameterizations

As discussed in an earlier section, complexity is not always a desirable feature of a model, as over-fitting becomes a possibility. Representing a simpler form of sediment model, two oxygen flux parameterizations were optimized to observations using a non-linear regression, and their resulting output compared to that of the layered models. Their fit was

inferior to that of the layered models; however, a simple analysis of their behaviour was very revealing about how the sediment oxygen fluxes behaved in the MERL systems.

While there obviously exists a relationship between an oxygen influx and the overlying oxygen concentration, such that consumption decreases as oxygen approaches zero, figure 3.13 clearly indicates an increase of sediment oxygen uptake with decreasing oxygen concentrations within the MERL mesocosms. This likely occurs as a result of seasonality in the two signals: high overlying O_2 during the winter-spring diatom bloom and high oxygen demand during the summer. As a result, the *Murrell and Lehrter* (2010) parameterization (ML10) proves to be completely out of phase with the observations (Fig 3.14). Indeed, this parameterization allowed to use a negative slope with a non-zero y-intercept, the output improved considerably, and was no longer out of phase, however such a parameterization clearly would not produce accurate oxygen fluxes in the limit that O_2 appraoaches zero. The *Hetland and DiMarco* (2008) parameterization (HD08) is much more successful, albeit entirely due to its ability to vary flux rates with seasonal temperatures. Oxygen concentrations contributed nothing to this parameterization's predictions, as the optimization process completely eliminated its oxygen sensitivity (Fig 3.13), effectively reducing the HD08 parameterization to the Arrhenius equation. Interestingly, after considering the cost function error resulting from observational uncertainty, this model performs only marginally worse than the two- and multi-layer models, which both share very similar temperature-scaling factors in their calculation of carbon metabolism rates. It is worth noting that while the HD08 model was fit only to oxygen fluxes, the layered models were also fit to other observations, requiring some compromise to their oxygen fluxes and putting them at a disadvantage. Furthermore, the time-invariant POM flux inputs may have nullified a significant advantage of the layered models, as they no longer were able to exploit the full dynamics of carbon storage, but instead accumulated and metabolized carbon according to temperature trends only.

That a parameterization as simple as that of the HD08 should behave so similarly to the layered models in terms of its oxygen flux demonstrates that given the right conditions, simple models can be of value. This model also demonstrates the critical importance of representing temperature sensitivity within the sediment, as it alone is able to represent the majority of the variation within oxygen fluxes. For this experiment, the HD08 parameterization used a single parameter across all the mesocosms to describe its behaviour.

Had each mesocosm received its own parameter (as did the layered models' POM flux parameterizations), this model would have done even better.

4.4 Cross Validation

The cross validation experiment is a test of a model's ability to adapt to new environments without any adjustment of its parameters. This was done by optimizing a model in a set of randomly chosen mesocosms and using the resulting parameter set to run the model in all the mesocosms. If a model is, on average, able to keep its cost function below its initial cost value, one can conclude that optimization of a model to the observations of one environment tends also to improve its fit to some other environments. It is also possible to compare the average cost of different models to gauge which of the two is better suited to general application. The multi-layer model seemed to be quite versatile, as it managed an average cost of 3.37 ± 2.8, which is lower but within the margin of error than the baseline value of 4. It also generally had a smaller cost than the two-layer model which didn't manage to stay below the baseline, scoring an average cost of 4.08 ± 2.8. While the uncertainties associated with these scores are very large, a consistent result was achieved when costs were re-evaluated without the eutrophic mesocosms cost contributions. These costs, 0.40 ± 0.03 for the multi-layer model and 0.57 ± 0.03 for the two-layer model, again favoured the multi-layer model, this time outside the bounds of uncertainty.

This result suggests that the multi-layer model has better predictive abilities, and this reinforces a prior finding: initial optimizations of the model produced small cost functions, regardless of whether noisy data from the eutrophic mesocosms were used in the optimization. Essentially this is partly the result of the multi-layer model's chemistry parameters being insensitive. The model is less reliant on specific parameter values and, instead, is more responsive to the surrounding chemical concentrations.

The oxygen flux cross validation experiments included the HD08 parameterizations, which utilized temperature to scale its rate of oxygen uptake. The multi-layer model proved to be the most versatile, with an average oxygen cost contribution of $0.70 \pm .04$. The HD08 fared the same, although its average cost was a little bit larger ($0.83 \pm .04$), and the two-layer model fared the worst ($1.11 \pm .04$), its average cost being larger than its starting value. The success of the multi-layer model to adequately function in different mesocosms without parameter adjustment suggests either that this model is less prone to

overfitting than the two-layer model, or that it is a better design than the two-layer model, or both.

While it is difficult to identify which aspect of the two-layer model may be suffering from an excess of parameterization, it is true that the two-layer model parameterizes a number of phenomena that the multi-layer model simulates explicitly. For example, prior discussion has mentioned how the two-layer model produces an oxygen sensitive rate of denitrification by using an aerobic and an anaerobic rate constant. Another example is the two-layer model's estimation of the thickness of the aerobic layer. This calculation diffuses oxygen from the overlying water into the sediment with a diffusion rate parameter Dd0, and a temperature sensitivity factor thetaDd0. At the same time, a different pair of parameters, MixPW and thtaDd, govern the temperature sensitive diffusion between the two sediment layers. In contrast, the multi-layer model uses only one pair of parameters, diffusion parameter, D, and the temperature factor theta Dpw to govern diffusion between all of the layers. Interestingly, most of the parameters mentioned above (kapp1no3s, Dd0, MixPW, and thtaDp) were included in the optimization and are possible candidates for overfitting in the two-layer model.

CHAPTER 5

CONCLUSION

Using observations of sediment fluxes and water chemistry from eutrophication experiments performed at MERL, I was able to optimize and compare two qualitatively different sediment models: a vertically integrated two-layer model and a vertically resolved multi-layer model. Modelling sediment fluxes in the MERL system required model inputs of a depositional flux of particulate organic matter (POM flux) which was not observed during the experiments. The POM fluxes were consequently parameterized in a number of ways. Generally, the models were most successful when the POM fluxes were set to constant rates, rather than scaling the flux with water column biomass, a surprising conclusion, considering that the majority of water column models use the latter kind of parameterizations. Some of the more eutrophic mesocosms had very noisy observations, however, and this likely interfered with the sediment model optimization process. When data from the eutrophic mesocosms were not used to evaluate model performance, it sometimes became easier to compare the performance of the two models. The multi-layer model generally performed better, achieving smaller misfits, while also better representing other systems without readjusting its parameters. The superior performance of the multi-layer model is thought to result from its ability to resolve phenomena which the two-layer model is required to parameterize. Denitrification, for example is highly dependent on the spatial distribution of oxygen and nitrogen in the multi-layer model, while this spatial variation is parameterized in the two-layer model. As a result, the two-layer model may be more prone to overfitting. Finally, two oxygen flux parameterizations were compared with the two-layer models. One such temperature sensitive paremeterization, while not as versatile

as the more complex layered models, generated reasonably accurate oxygen fluxes, and demonstrated the utility of simple models under certain conditions.

APPENDIX A

OPTIMIZED PARAMETER VALUES

Table A.1: Two-layer model parameter names, description, initial value, and final value after optimization from the full dataset, including uncertainty. Correlated and insensitive parameters were identified using the Hessian matrix, and were not optimized. The inverse of the Hessian matrix only approximates the covariance matrix of a model, therefore the uncertainties are only estimates.

Parameter	Description	Base value	Result	Units
D_T	Sediment temperature Diffusion Rate	1.8×10^{-3}	$1.7\pm5.0 \times 10^{-4}$	$\frac{cm^2}{d}$
$r_{\mathrm{met},1}$	Carbon decomposition rate, lability class 1	3.5×10^{-2}	Correlated	$\frac{1}{\mathrm{day}}$
$r_{\mathrm{met},2}$	Carbon decomposition rate, lability class 2	1.8×10^{-3}	Correlated	$\frac{1}{\mathrm{day}}$
$r_{\mathrm{met},3}$	Carbon decomposition rate, lability class 3	1.0×10^{-6}	Insensitive	$\frac{1}{\mathrm{day}}$
$\theta_{\mathrm{met},1}$	Carbon metab. rate, temperature factor, lability class 1	1.10	Correlated	-

Continued on next page

Table A.1 – continued from previous page

Parameter	Description	Value	Result	Units
$\theta_{\mathrm{met,2}}$	Carbon metab. rate, temperature factor, lability class 2	1.15	Correlated	-
$\theta_{\mathrm{met,3}}$	Carbon metab. rate, temperature factor, lability class 3	1.17	Insensitive	-
L_{sed}	Burial mass transfer coefficient	2.5×10^{-1}	Correlated	$\frac{\mathrm{cm}}{\mathrm{year}}$
D_{s}	Particle diffusion rate	6.0×10^{-5}	Correlated	$\frac{\mathrm{cm}^2}{\mathrm{d}}$
D_{pw}	Porewater diffusion rate	2.5×10^{-3}	$7.2\pm6.7\times10^{-3}$	$\frac{\mathrm{cm}^2}{\mathrm{d}}$
θ_{D_s}	Particle mixing velocity temperature factor	1.117	1.130 ± 0.063	-
$\theta_{D_{pw}}$	Porewater mixing velocity temperature factor	1.08	1.137 ± 0.059	-
$D_{\mathrm{s}}0$	Surface porewater mixing velocity	1.2×10^{-3}	$3.22\pm0.001\times10^{-5}$	$\frac{\mathrm{cm}^2}{\mathrm{d}}$
$\theta_{\mathrm{D_{pw}0}}$	Surface porewater mixing velocity temperature factor	1.08	Correlated	-
κ_{nit}	Nitrification reaction velocity	1.31×10^{-1}	$1.35\pm0.57\times10^{-1}$	$\frac{\mathrm{m}}{\mathrm{d}}$
$\pi_{\mathrm{NH_4}}$	Ammonia partitioning	1.0	$1.6\pm14.0\times10^{-2}$	$\frac{\mathrm{L}}{\mathrm{kg}}$
θ_{nit}	Nitrification, ammonia half saturation	1.12	1.00 ± 0.18	-
$\theta_{\mathrm{k,nit,NH_4}}$	Nitrification, ammonia half saturation temperature factor	1.125	Correlated	-
k_{nit,NH_4}	Nitrification, ammonia half saturation	7.28×10^{2}	Correlated	$\frac{\mu\mathrm{gN}}{\mathrm{L}}$
$\kappa_{\mathrm{dnf,1}}$	Denitrification rate, aerobic	1.0×10^{-1}	$8.3\pm4.9\times10^{-2}$	$\frac{\mathrm{m}}{\mathrm{d}}$
$k_{\mathrm{dnf,2}}$	Denitrification rate, anaerobic	2.5×10^{-1}	Correlated	$\frac{\mathrm{m}}{\mathrm{d}}$
θ_{dnf}	Denitrification rate, temperature factor	2.5×10^{-1}	Correlated	-

Continued on next page

Table A.1 – continued from previous page

Parameter	Description	Value	Result	Units
$\kappa_{\mathrm{H_2Sox,aq}}$	Dissolved Sulfide reaction velocity, aerobic	2.0×10^{-1}	Insensitive	$\frac{\mathrm{m}}{\mathrm{d}}$
$\kappa_{H_2Sox,s}$	Particulate Sulfide reaction velocity, anaerobic	4.0×10^{-1}	Insensitive	$\frac{\mathrm{m}}{\mathrm{d}}$
$\pi_{H_2S,1}$	H_2S partitioning, aerobic	1.0×10^{2}	Insensitive	$\frac{\mathrm{L}}{\mathrm{kg}}$
$\pi_{H_2S,2}$	H_2S partitioning, anaerobic	1.0×10^{2}	Correlated	$\frac{\mathrm{L}}{\mathrm{kg}}$
θ_{H_2Sox}	H_2S reaction velocity temperature factor	1.08	Insensitive	-
k_{H_2Sox,O_2}	H_2S oxidation, half O_2 saturation	4.0	Insensitive	$\frac{\mathrm{mgO_2}}{\mathrm{L}}$
$\pi_{PO_4,base}$	Phosphate partitioning base	2.0×10^{1}	5.6 $\pm$5.3	$\frac{\mathrm{L}}{\mathrm{kg}}$
$\pi_{PO_4,exp}$	Phosphate partitioning, O_2 sensitivity	2.0×10^{1}	Correlated	$\frac{\mathrm{L}}{\mathrm{kg}}$
$[O_2]_{\mathrm{crit}}$	Hypoxic phosphorus storage threshold	2.0	Insensitive	$\frac{\mathrm{mgO_2}}{\mathrm{L}}$
$k_{\mathrm{Ds,O_2}}$	Particle mixing O_2 half saturation	4.0	4.0 $\pm$14.3	$\frac{\mathrm{mgO_2}}{\mathrm{L}}$
T_{bnth}	Bioturbation temperature threshold	1.0×10^{1}	1.2 $\pm$ 4.5	°C
k_{s}	Benthic stress decay rate	3.0×10^{-2}	Correlated	$\frac{1}{\mathrm{d}}$
$D_{\mathrm{s,min}}$	Minimum bioturbation	3.0×10^{-6}	Correlated	$\frac{\mathrm{cm^2}}{\mathrm{d}}$
$\kappa_{\mathrm{CH_4ox}}$	Methane oxidation reaction velocity	2.0×10^{-1}	Insensitive	$\frac{\mathrm{m}}{\mathrm{d}}$
$\theta_{\mathrm{CH_4ox}}$	Methate oxidation temperature factor	1.08	Insensitive	-
$k_{\mathrm{CH_4ox,O_2}}$	Methane oxidation, oxygen half saturation	2.0×10^{-1}	Insensistive	$\frac{\mathrm{mgO_2}}{\mathrm{L}}$
$k_{\mathrm{sul,SO_4}}$	Methane production, sulphate half saturation	1.0×10^{-1}	Insensitive	$\frac{\mathrm{mgS}}{\mathrm{L}}$

Continued on next page

Table A.1 – continued from previous page

Parameter	Description	Value	Result	Units
p_{const}CO1	POM depositional flux, C01	8.29×10^{2}	$9.54\pm.75 \times 10^{2}$	$\frac{\mu\text{molC}}{\text{cm}^2\text{yr}}$
p_{const}CO5	POM depositional flux, C05	8.29×10^{2}	$8.69\pm.71 \times 10^{2}$	$\frac{\mu\text{molC}}{\text{cm}^2\text{yr}}$
p_{const}CO8	POM depositional flux, C08	8.29×10^{2}	$1.18\pm.81 \times 10^{3}$	$\frac{\mu\text{molC}}{\text{cm}^2\text{yr}}$
p_{const}01X	POM depositional flux, 01X	1.12×10^{3}	$1.55\pm.86 \times 10^{3}$	$\frac{\mu\text{molC}}{\text{cm}^2\text{yr}}$
p_{const}02X	POM depositional flux, 02X	1.03×10^{3}	$1.35\pm.69 \times 10^{3}$	$\frac{\mu\text{molC}}{\text{cm}^2\text{yr}}$
p_{const}04X	POM depositional flux, 04X	1.60×10^{3}	$1.65\pm.57 \times 10^{3}$	$\frac{\mu\text{molC}}{\text{cm}^2\text{yr}}$
p_{const}08X	POM depositional flux, 08X	1.62×10^{3}	$1.89\pm.74 \times 10^{3}$	$\frac{\mu\text{molC}}{\text{cm}^2\text{yr}}$
p_{const}16X	POM depositional flux, 16X	2.02×10^{3}	$2.64\pm.77 \times 10^{3}$	$\frac{\mu\text{molC}}{\text{cm}^2\text{yr}}$
p_{const}32X	POM depositional flux, 32X	2.15×10^{3}	$1.77\pm.51 \times 10^{3}$	$\frac{\mu\text{molC}}{\text{cm}^2\text{yr}}$

Table A.2: Multi-layer model parameter names, function, initial value, and final value after optimization from the full dataset. Correlated and insensitive parameters were identified using the Hessian matrix, and were not optimized. The inverse of the Hessian matrix only approximates the covariance matrix of a model, therefore the uncertainties are only estimates.

Parameter	Description	Value	Result	Units
D_{pw}	Porewater Diffusion Rate	1.5	1.03 ± 0.66	$\frac{\text{cm}^2}{\text{d}}$
p_{const}C01	POM depositional flux, C01	$6.858\pm \times 10^{2}$	$1.01\pm0.8\times10^{3}$	$\frac{\mu\text{mol}}{\text{cm}^2\text{yr}}$
p_{const}C05	POM depositional flux, C05	6.450×10^{2}	$6.72\pm0.8\times10^{2}$	$\frac{\mu\text{mol}}{\text{cm}^2\text{yr}}$
p_{const}C08	POM depositional flux, C08	7.251×10^{2}	$1.16\pm0.8\times10^{2}$	$\frac{\mu\text{mol}}{\text{cm}^2\text{yr}}$
p_{const}01X	POM depositional flux, 01X	1.184×10^{3}	$1.23\pm1.0\times10^{2}$	$\frac{\mu\text{mol}}{\text{cm}^2\text{yr}}$
p_{const}02X	POM depositional flux, 02X	8.284×10^{2}	$1.11\pm0.9\times10^{2}$	$\frac{\mu\text{mol}}{\text{cm}^2\text{yr}}$

Continued on next page

Table A.2 – continued from previous page

Parameter	Description	Value	Result	Units
p_{const}04X	POM depositional flux, 04X	1.002×10^{3}	$1.11\pm0.7\times10^{2}$	$\frac{\mu\text{mol}}{\text{cm}^2\text{yr}}$
p_{const}08X	POM depositional flux, 08X	1.688×10^{3}	$1.75\pm1.0\times10^{2}$	$\frac{\mu\text{mol}}{\text{cm}^2\text{yr}}$
p_{const}16X	POM depositional flux, 16X	1.401×10^{3}	$2.49\pm1.2\times10^{2}$	$\frac{\mu\text{mol}}{\text{cm}^2\text{yr}}$
p_{const}32X	POM depositional flux, 32X	1.580×10^{3}	$1.75\pm0.9\times10^{2}$	$\frac{\mu\text{mol}}{\text{cm}^2\text{yr}}$
H_{bio}	Depth of bioturbated layer	5.0	Insensitive	cm
D_s	Bioturbation "diffusivity"	1.53	$8.29\pm8.4\times10^{-1}$	$\frac{\text{cm}^2}{\text{yr}}$
$D_{\text{s,coeff}}$	Bioturbation dropoff below zbio	1.0	Insensitive	$\frac{1}{\text{cm}}$
$r_{\text{met,1}}$	Remineralization rate for inert organic matter	2.00×10^{-2}	$5.93\pm7.6\times10^{-2}$	$\frac{1}{\text{yr}}$
$r_{\text{met,2}}$	Remineralization rate for labile organic matter	2.0	6.0 ± 4.8	$\frac{1}{\text{yr}}$
$k_{\text{aer,O}_2}$	Aerobic remineralization, O_2 half saturation	3.0	Insensitive	$\frac{\mu\text{molO}_2}{\text{L}}$
$k_{\text{anox,O}_2}$	Anaerobic remineralization, inhibition by O_2	3.0	Insensitive	$\frac{\mu\text{molO}_2}{\text{L}}$
r_{ODUox}	ODU redox max rate	2.0×10^{1}	$2.0\pm1.2\times10^{1}$	$\frac{1}{\text{d}}$
$k_{\text{ODUox,O}_2}$	ODU redox, O_2 half saturation	3.0	Insensitive	$\frac{\mu\text{molO}_2}{\text{L}}$
r_{nit}	Nitrification max rate	2.0×10^{1}	$2.2\pm1.1\times10^{1}$	$\frac{1}{\text{d}}$
$k_{\text{nit,O}_2}$	Nitrification, O_2 half saturation	1.0	Insensitive	$\frac{\mu\text{molO}_2}{\text{L}}$
$k_{\text{dnf,NO}_3}$	Denitrification, NO_3 half saturation	3.0×10^{1}	Insensitive	$\frac{\mu\text{molNO}_3}{\text{L}}$
k_{dnf,O_2}	O_2 Denitrification, inhibition by O_2	1.0×10^{1}	Insensitive	$\frac{\mu\text{molO}_2}{\text{L}}$
$k_{\text{anox,NO}_3}$	Anaerobic remineraliztion, inhibition by NO_3	5.0	Insensitive	$\frac{\mu\text{molNO}_3}{\text{L}}$
r_{amx}	Anammox max rate	4.0×10^{-1}	Insensitive	$\frac{1}{\text{d}}$

Continued on next page

Table A.2 – continued from previous page

Parameter	Description	Value	Result	Units
k_{amx,NO_3}	Anammox NO_3 saturation	3.0	Insensitive	$\frac{\mu\text{molNO}_3}{\text{L}}$
k_{amx,O_2}	Anammox inhibition by O_2	1.0×10^{-2}	Insensitive	$\frac{\mu\text{molO}_2}{\text{L}}$
$\pi_{\text{po4,exp}}$	Phosphate storage partition, oxygen sensitivity factor	1.2	Correlated	$\frac{\text{L}_{\text{solid}}}{\text{L}_{\text{total}}}$
$\pi_{\text{po4,base}}$	Phosphate storage partition, base	2.0	Correlated	-
$[O_2]_{\text{crit}}$	Phosphate storage, critical O_2 concentration	6.25	Correlated	$\frac{\mu\text{molO}_2}{\text{L}}$
$\theta_{\text{met,1}}$	Inert organic matter remineralization, temperature factor	1.1	Correlated	-
$\theta_{\text{met,2}}$	Labile organic matter remineralization, temperature factor	1.1	1.09 ± 0.07	-
$\theta_{\text{D}_{\text{pw}}}$	Porewater diffusion, temperature factor	1.1	1.1 ± 0.1	-
$\theta_{\text{D}_{\text{s}}}$	Bioturbation, temperature factor	1.1	1.2 ± 0.7	-

APPENDIX B

OPTIMIZED MODEL COST VALUES

Table B.1: Overall Cost Contributions

Model	Cost: including eutrophic mesocosm contributions	Cost: ignoring eutrophic mesocosm contributions	**C**, Cost: optimized without eutrophic mesocosms entirely
Two-Layer Model	3.09±2.84	.85±.03	.68±.03
Multi-Layer Model	3.11±2.84	.52±.04	.51±.03

BIBLIOGRAPHY

Bagniewski, W., K. Fennel, M. Perry, and E. D'Asaro, Optimizing models of the North Atlantic spring bloom using physical, chemical and bio-optical observations from a Lagrangian float, *Biogeosciences*, *8*, 1291–1307, 2011.

Berg, P., N. Risgaard-Petersen, and S. Rysgaard, Interpretation of measured concentration profiles in sediment pore water, *Limnology and Oceanography*, pp. 1500–1510, 1998.

Berner, R., *Early diagenesis: A theoretical approach*, 1, Princeton Univ Pr, 1980.

Boesch, D., R. Brinsfield, and R. Magnien, Chesapeake bay eutrophication: Scientific understanding, ecosystem restoration, and challenges for agriculture, *J. Environ. Qual*, *30*, 303–320, 2001.

Boström, B., J. Andersen, S. Fleischer, and M. Jansson, Exchange of phosphorus across the sediment-water interface, *Hydrobiologia*, *170*, 229–244, 1988.

Boudreau, B., *Diagenetic models and their implementation: modelling transport and reactions in aquatic sediments*, Springer New York, 1997.

DiToro, D., *Sediment flux modeling.*, Wiley-Interscience, 2001.

Fennel, K., M. Losch, J. Schroter, and M. Wenzel, Testing a marine ecosystem model: sensitivity analysis and parameter optimization, *Journal of Marine Systems*, *28*, 45–63, 2001.

Fennel, K., J. Wilkin, J. Levin, J. Moisan, J. OReilly, and D. Haidvogel, Nitrogen cycling in the Middle Atlantic Bight: Results from a three-dimensional model and implications for the North Atlantic nitrogen budget, *Global Biogeochemical Cycles*, *20*, GB3007, 2006.

Fennel, K., et al., Modeling denitrification in aquatic sediments, *Biogeochemistry*, *93*, 159–178, 2009.

Fitzpatrick, J., A users guide for RCA: release 3.0, *Tech. rep.*, HydroQual Inc, Magwag, New Jersey, 2004.

Friedrichs, M., et al., Assessment of skill and portability in regional marine biogeochemical models: Role of multiple planktonic groups, *J. Geophys. Res*, *112*, C08001, 2007.

Frithsen, J., A. Keller, and M. Pilson, Effects of inorganic nutrient additions in coastal areas: a mesocosm experiment data report. Volume 1. MERL Series, *Tech. rep.*, University of Rhode Island, 1985a.

Frithsen, J., A. Keller, and M. Pilson, Effects of inorganic nutrient additions in coastal areas: a mesocosm experiment data report. Volume 2. MERL Series, *Tech. rep.*, University of Rhode Island, 1985b.

Frithsen, J., A. Keller, and M. Pilson, Effects of inorganic nutrient additions in coastal areas: a mesocosm experiment data report. Volume 3. MERL Series, *Tech. rep.*, University of Rhode Island, 1985c.

Hetland, R., and S. DiMarco, How does the character of oxygen demand control the structure of hypoxia on the Texas-Louisiana continental shelf?, *Journal of Marine Systems*, *70*, 49–62, 2008.

Kelly, J., V. Berounsky, S. Nixon, and C. Oviatt, Benthic-pelagic coupling and nutrient cycling across an experimental eutrophication gradient, *Marine Ecology Progress Series*, *26*, 207–219, 1985.

Kemp, W., P. Sampou, J. Caffrey, M. Mayer, K. Henriksen, and W. Boynton, Ammonium recycling versus denitrification in Chesapeake Bay sediments, *Limnology and Oceanography*, pp. 1545–1563, 1990.

Kemp, W., P. Sampou, J. Garber, J. Tuttle, and W. Boynton, Seasonal depletion of oxygen from bottom waters of Chesapeake Bay: Roles of benthic and planktonic respiration and physical exchange processes., *Marine Ecology Progress Series. Oldendorf*, *85*, 137–152, 1992.

Kemp, W., et al., Eutrophication of Chesapeake Bay: historical trends and ecological interactions, *Marine Ecology Progress Series*, *303*, 1–29, 2005.

Mattern, J. P., Ensemble-based data assimilation for a physical-biological ocean model near Bermuda, Master's thesis, Universität zu Lübeck, 2008.

Middelburg, J., K. Soetaert, P. Herman, and C. Heip, Denitrification in marine sediments: A model study., *Global Biogeochemical Cycles*, *10*, 1996.

Murrell, M., and J. Lehrter, Sediment and lower water column oxygen consumption in the seasonally hypoxic region of the Louisiana continental Shelf, *Estuaries and Coasts*, pp. 1–13, 2010.

Oviatt, C., M. Pilson, S. Nixon, J. Frithsen, D. Rudnick, J. Kelly, J. Grassle, and J. Grassle, Recovery of a polluted estuarine system: a mesocosm experiment., *Marine ecology progress series. Oldendorf*, *16*, 203–217, 1984.

Oviatt, C., D. Rudnick, A. Keller, P. Sampou, and G. Almquist, A comparison of system (O_2, and CO_2,) and C-14 measurements of metabolism in estuarine mesocosms, *Mar. Ecol. Prog. Ser*, *2*, 57–67, 1986.

Seitzinger, S., J. Harrison, J. Böhlke, A. Bouwman, R. Lowrance, B. Peterson, C. Tobias, and G. Drecht, Denitrification across landscapes and waterscapes: a synthesis, *Ecological Applications*, *16*, 2064–2090, 2006.

Soetaert, K., P. Herman, and J. Middelburg, A model of early diagenetic processes from the shelf to abyssal depths, *Geochimica et Cosmochimica Acta*, *60*, 1019–1040, 1996a.

Soetaert, K., P. Herman, and J. Middelburg, Dynamic response of deep-sea sediments to seasonal variations: A model, *Limnology and Oceanography*, pp. 1651–1668, 1996b.

Soetaert, K., P. Herman, J. Middelburg, C. Heip, T. van Weering, E. Epping, and W. Helder, Modeling ^{210}Pb-derived mixing activity in ocean margin sediments: diffusive versus nonlocal mixing, *Journal of Marine Research*, *54*, 1207–1227, 1996c.

Soetaert, K., J. Middelburg, P. Herman, and K. Buis, On the coupling of benthic and pelagic biogeochemical models, *Earth-Science Reviews*, *51*, 173–201, 2000.

Thacker, W., The role of the Hessian matrix in fitting models to measurements, *Journal of Geophysical Research*, *94*, 6177–6196, 1989.